Axion Field and the Quark Nugget's Formation at the QCD Phase Transition

by

Xunyu Liang

B.Sc., University of Victoria, 2014

A THESIS SUBMITTED IN PARTIAL FULFILLMENT OF
THE REQUIREMENTS FOR THE DEGREE OF

MASTER OF SCIENCE

in

The Faculty of Graduate and Postdoctoral Studies

(Physics)

THE UNIVERSITY OF BRITISH COLUMBIA

(Vancouver)

August 2016

Abstract

We study a testable dark matter (DM) model outside of the standard WIMP paradigm in which the observed ratio $\Omega_{\rm dark} \simeq \Omega_{\rm visible}$ for visible and dark matter densities finds its natural explanation as a result of their common QCD origin when both types of matter (DM and visible) are formed at the QCD phase transition and both are proportional to $\Lambda_{\rm QCD}$. Instead of the conventional "baryogenesis" mechanism we advocate a paradigm when the "baryogenesis" is actually a charge separation process which occur in the presence of the $\mathcal{CP}$ odd axion field $a(x)$. In this scenario the global baryon number of the Universe remains zero, while the unobserved antibaryon charge is hidden in form of heavy nuggets, similar to Witten's strangelets and compromise the DM of the Universe.

In the present work we study in great detail a possible formation mechanism of such macroscopically large heavy objects. We argue that the nuggets will be inevitably produced during the QCD phase transition as a result of Kibble-Zurek mechanism on formation of the topological defects during a phase transition. Relevant topological defects in our scenario are the closed bubbles made of the $N_{\rm DW} = 1$ axion domain walls. These bubbles, in general, accrete the baryon (or antibaryon) charge, which eventually result in formation of the nuggets and anti-nuggets carrying a huge baryon (antibaryon) charge. A typical size and the baryon charge of these macroscopically large objects is mainly determined by the axion mass m_a. However, the main consequence of the model, $\Omega_{\rm dark} \approx \Omega_{\rm visible}$ is insensitive to the axion mass which may assume any value within the observationally allowed window $10^{-6}{\rm eV} \lesssim m_a \lesssim 10^{-3}{\rm eV}$. We also estimate the baryon to entropy ratio $\eta \equiv n_B/n_\gamma \sim 10^{-10}$ within this scenario. Finally, we comment on implications of these results to the axion search experiments, including microwave cavity and the Orpheus experiments.

Preface

The results of this thesis has been published on arXiv as Xunyu Liang and Ariel Zhitnitsky, arXiv:1606.00435 [hep-ph].

Section 2.4 and appendices were my work, but also being improved by Ariel Zhitnitsky, especially Appendix A, into a more logical framework. Additionally, the inclusion of the viscosity term was suggested by me. The rest of new results, chapter 2, 3, and 5, presented in this thesis was done and written by Ariel Zhitnitsky. Also, the remaining review chapters were written by Ariel Zhitnitsky.

Table of Contents

Appendices

List of Tables

List of Figures

Acknowledgements

I would like to thank my supervisor, Professor Ariel Zhitnitsky. Starting with little experience, he guided me into research, and finally allowed this thesis to be my own work, despite the fact the most difficult problems were solved by him. Also, he is always pleasant to give support when I had problems in physics, conference, and research. All of his effort and patience are sincerely appreciated.

I also want to thank Kyle Lawson, an intelligent postdoctoral fellow in our research group, who is willing to spend a great amount of time to review my thesis and give so many careful and insightful comments.

Chapter 1

Introduction

Very recently, at the time of the thesis is being written, the world's most sensitive dark matter (DM) detector – LUX (the Large Underground Xenon DM experiment) completes its nearly 2-year search. However, similar to other long-term searches, it hardly provides evidence [1] to support the existence of WIMPs (Weakly Interacting Massive Particles), a prevailing DM model. The lack of signals may hint an alternative DM model could be favorable.

As one of the motivations, this thesis presents a simple composite object, namely quark nugget, that can be served as an alternative DM candidate. Even better, these little compact nuggets may solve another unsolved fundamental problem – the baryon asymmetry.

1.1 Two sides of the same coin

The origin of the observed asymmetry between matter and antimatter is one of the largest open questions in cosmology. The nature of the dark matter is another open question in cosmology. In this thesis we advocate an idea that these two, apparently unrelated, problems are in fact two sides of the same coin. Furthermore, both mysterious effects are originated at one and the same cosmological epoch from one and the same QCD physics. Normally, it is assumed that the majority of dark matter is represented by a new fundamental field coupled only weakly to the standard model particles, these models may then be tuned to match the observed dark matter properties. We take a different perspective and consider the possibility that the dark matter is in fact composed of well known quarks and antiquarks but in a new high density phase, similar to the Witten's strangelets, see original work [2] and some related studies [3].

There are few new crucial elements in proposal [4, 5], in comparison with previous studies [2, 3]. First of all, the nuggets could be made of matter as well as antimatter in our framework as a result of separation of charges, see few comments below. Secondly, the stability of the DM nuggets is provided by the axion domain walls with extra pressure, in contrast with

original studies when stability is assumed to be achieved even in vacuum, at zero external pressure. Finally, an overall coherent baryon asymmetry in the entire Universe is a result of the strong CP violation due to the fundamental θ parameter in QCD which is assumed to be nonzero at the beginning of the QCD phase transition. This source of strong CP violation is no longer available at the present epoch as a result of the axion dynamics, see original papers [6–8] and recent reviews [9–16] on the subject. We highlight the basics ideas of this framework in the present Introduction, while we elaborate on these new crucial elements in details in section 2.1.

It is generally assumed that the universe began in a symmetric state with zero global baryonic charge and later (through some baryon number violating process) evolved into a state with a net positive baryon number. As an alternative to this scenario we advocate a model in which "baryogenesis" is actually a charge separation process in which the global baryon number of the universe remains zero. In this model the unobserved antibaryons come to comprise the dark matter. A connection between dark matter and baryogenesis is made particularly compelling by the similar energy densities of the visible and dark matter with $\Omega_{\rm dark} \simeq 5 \cdot \Omega_{\rm visible}$. If these processes are not fundamentally related the two components could exist at vastly different scales.

In the model [4, 5] baryogenesis occurs at the QCD phase transition. Both quarks and antiquarks are thermally abundant in the primordial plasma but, in addition to forming conventional baryons, some fraction of them are bound into heavy nuggets of quark matter in a colour superconducting phase (an analogous phase to superconductors in condensed matter). Nuggets of both matter and antimatter are formed as a result of the dynamics of the axion domain walls as originally proposed in refs.[4, 5]. A number of very hard dynamical questions in strongly coupled QCD which are related to the nuggets's formation have not been studied in any details in the original papers. The main goal of the present work is to make the first step in the direction to address these hard questions.

If the fundamental θ parameter were identically zero at the QCD phase transition in early universe, an equal number of nuggets made of matter and antimatter would be formed. It would result in vanishing of the visible baryon density at the present epoch. However, the fundamental CP violating processes associated with the θ term in QCD (which is assumed to be small, but still non-zero at the very beginning of the QCD phase transition) results in the preferential formation of anti-nuggets over the nuggets. This preference is essentially determined by the dynamics of coherent axion field $\theta(x)$ at the initial stage of the nugget's formation. The resulting asymmetry

is not sensitive to a small magnitude of the axion field $\theta(x)$ at the QCD phase transition as long as it remains coherent on the scale of the Universe, see chapter 3 for the details.

The remaining antibaryons in the plasma then annihilate away leaving only the baryons whose antimatter counterparts are bound in the excess of anti-nuggets and thus unavailable to annihilate. All asymmetry effects are order of one, irrespectively to the magnitude of $\theta(x)$ at the moment of formation. This is precisely the main reason of why the visible and dark matter densities must be the same order of magnitude

$$\Omega_{\rm dark} \approx \Omega_{\rm visible} \tag{1.1}$$

as they both proportional to the same fundamental $\Lambda_{\rm QCD}$ scale, and they both are originated at the same QCD epoch. In particular, if one assumes that the nuggets and anti-nuggets saturate the dark matter density than the observed matter to dark matter ratio $\Omega_{\rm dark} \simeq 5 \cdot \Omega_{\rm visible}$ corresponds to a specific proportion when number of anti-nuggets is larger than number of nuggets by a factor of $\sim 3/2$ at the end of nugget's formation. This would result in a matter content with baryons, quark nuggets and antiquark nuggets in an approximate ratio

$$|B_{\rm visible}| : |B_{\rm nuggets}| : |B_{\rm antinuggets}| \simeq 1 : 2 : 3, \tag{1.2}$$

with no net baryonic charge. If these processes are not fundamentally related the two components $\Omega_{\rm dark}$ and $\Omega_{\rm visible}$ could easily exist at vastly different scales.

Though the QCD phase diagram at $\theta \neq 0$ as a function of T and μ is basically unknown, it is well understood that θ is in fact the angular variable, and therefore supports various types of the domain walls, including the so-called $N_{DW} = 1$ domain walls[1] when θ interpolates between one and the same physical vacuum state $\theta \to \theta + 2\pi$. Furthermore, it is expected that the closed bubbles made of these $N_{DW} = 1$ axion domain walls are also produced during the QCD phase transition with a typical wall tension $\sigma_a \sim m_a^{-1}$ where m_a is the axion mass. Precisely this scale determines the size and the baryon charge of the nuggets, see equations (1.3), (1.4) below.

The collapse of these close bubbles is halted due to the Fermi pressure acting inside of the bubbles. The crucial element which stops the collapse of the bubbles from complete annihilation is the presence of the QCD substructure inside the axion domain wall. This substructure forms immediately

[1] N_{DW} represents the phase difference between the two side of the end of a domain wall $\theta \to \theta + 2\pi N_{DW}$.

after the QCD phase transition as discussed in [4]. The equilibrium of the obtained nugget system has been analyzed in [4] for a specific axion domain wall tension within the observationally allowed window $10^{-6}\text{eV} \leq m_a \leq 10^{-3}\text{eV}$ consistent with the recent constraints [9–16]. It has been also argued in [4] that the equilibrium is typically achieved when the Fermi pressure inside the nuggets falls into the region when the colour superconductivity (CS) sets in[2].

The size and the baryon charge of the nuggets scale with the axion mass as follows

$$\sigma_a \sim m_a^{-1}, \quad R \sim \sigma_a, \qquad B \sim \sigma_a^3. \tag{1.3}$$

Therefore, when the axion mass m_a varies within the observationally allowed window $10^{-6}\text{eV} \lesssim m_a \lesssim 10^{-3}\text{eV}$ the nuggets parameters also vary as follows

$$10^{-6}\text{cm} \lesssim R \lesssim 10^{-3}\text{cm}, \quad 10^{23} \lesssim B \lesssim 10^{32}, \tag{1.4}$$

where the lowest axion mass $m_a \simeq 10^{-6}\text{eV}$ approximately[3] corresponds to the largest possible nuggets with $\langle B \rangle \simeq 10^{32}$. Variation of the axion mass by three orders of magnitude results in variation of the nugget's baryon charge by nine orders of magnitude according to relation (1.3). The corresponding allowed region is essentially unconstrained by present experiments, see details in section 1.2 below.

The fact that the CS may be realized in nature in the cores of neutron stars has been known for sometime [17, 18]. A new element which was advocated in proposal [4] is that a similar dense environment can be realized in nature due to the axion domain wall pressure playing a role of a "squeezer", similar to the gravity pressure in the neutron star physics.

Another fundamental ratio (along with $\Omega_{\text{dark}} \approx \Omega_{\text{visible}}$ discussed above) is the baryon to entropy ratio at present time

$$\eta \equiv \frac{n_B - n_{\bar{B}}}{n_\gamma} \simeq \frac{n_B}{n_\gamma} \sim 10^{-10}. \tag{1.5}$$

[2]There is no requirement for a first order phase transition (in contrast with original proposal [2]) for the bubble formation in this framework because the $N_{DW} = 1$ axion domain walls are formed irrespectively to the order of the phase transition. Needless to say that the phase diagram in general and the order of the phase transition in particular at $\theta \neq 0$ are still unknown because of the longstanding "sign problem" in the QCD lattice simulations at $\theta \neq 0$, see few comments and related references in chapter 5.

[3]There is no one-to-one correspondence between the axion mass m_a and the baryon charge of the nuggets B because for each given m_a there is an extended window of stable solutions describing different nugget's sizes [4].

If the nuggets were not present after the phase transition the conventional baryons and antibaryons would continue to annihilate each other until the temperature reaches $T \simeq 22$ MeV when the baryon density would be 9 orders of magnitude smaller than observed (1.5). This annihilation catastrophe, normally thought to be resolved as a result of "baryogenesis" was formulated by Sakharov[19], see also review [20]. In the framework of conventional baryogenesis, the ratio (1.5) is highly sensitive to many specific details of the models (for example, the general spectrum of the system, the coupling constants, and the particular strength of CP violation), see e.g. review[20].

In our proposal (in contrast with conventional frameworks on baryogenesis) this ratio is determined by a single parameter with a typical QCD scale, the formation temperature $T_{\rm form}$. This temperature is defined by a moment in evolution of the Universe when the nuggets and anti-nuggets basically have completed their formation and not much annihilation would occur at lower temperatures $T \leq T_{\rm form}$. The exact magnitude of temperature $T_{\rm form} \sim \Lambda_{\rm QCD}$ in our proposal is determined by many factors: transmission/reflection coefficients, evolution of the nuggets, expansion of the universe, cooling rates, evaporation rates, viscosity of the environment, the dynamics of the axion domain wall network, etc. All these effects are, in general, equally contribute to $T_{\rm form}$ at the QCD scale. Technically, the corresponding effects are hard to compute from the first principles as even basic properties of the QCD phase diagram at nonzero $\theta \neq 0$ are still unknown[4]. We plot three different conjectured cooling paths on Fig. 1.1.

However, the estimate of $T_{\rm form}$ up to factor 2 is quite a simple exercise as $T_{\rm form}$ must be proportional to the gap $\Delta \sim 100$ MeV when CS phase sets in inside the nuggets. The observed ratio (1.5) corresponds to $T_{\rm form} \simeq 40$ MeV, see [5] for the details. This temperature indeed represents a typical QCD scale, slightly below the critical temperature $T_{CS} \simeq 0.6\Delta \simeq 60$ MeV, according to standard estimates on colour superconductivity, see reviews [17, 18].

[4]The basic consequence (1.1) as well as (1.5) of this proposal are largely insensitive to the absolute value of the initial magnitude of the θ parameter. In other words, a fine tuning of the initial θ parameter is not required in this mechanism. The same comment (on "insensitivity" of the initial conditions) also applies to efficiency of the nugget's formation. This is because the baryon density at the present time is 10 orders of magnitude lower than the particle density at the QCD phase transition epoch according to the observations (1.5). Therefore, even a sufficiently low efficiency of the nugget's formation (still larger than 10^{-7}, see estimates in section 3.3) cannot drastically modify the generic relations (1.1), (1.5) due to a long evolution which eventually washes out any sensitivity to the initial conditions. The only crucial parameter which determines the final outcome (1.1), (1.5) is the formation temperature $T_{\rm form}$ as estimated below.

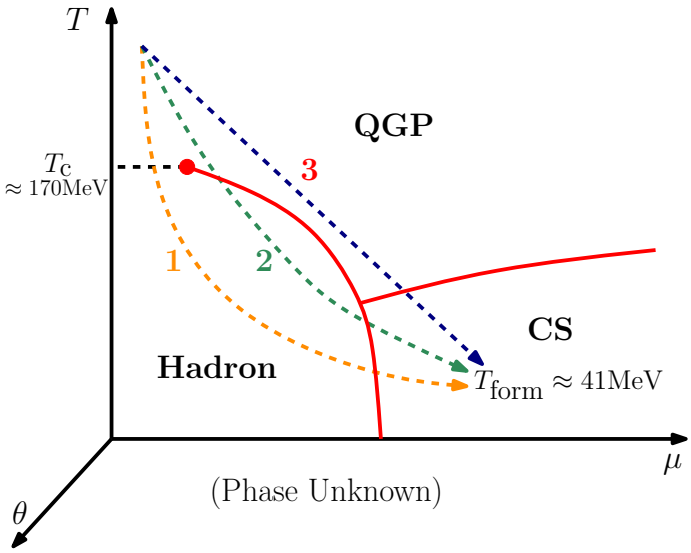

Figure 1.1: The conjectured phase diagram. Possible cooling paths are denoted as path 1, 2 or 3. The phase diagram is in fact much more complicated as the dependence on the third essential parameter, the θ is not shown as it is largely unknown. Therefore, the paths should be thought as lines in three dimensional parametrical space, not as lines on two-dimensional (μ, T) slice at $\theta = 0$ as shown on the present plot. It is assumed that the final destination after the nuggets are formed is the region with $T_{\rm form} \approx 41$ MeV, $\mu > \mu_c$ and $\theta \approx 0$, corresponding to the presently observed ratio (1.5), see text for the details.

Unlike conventional dark matter candidates, such as WIMPs the dark-matter/antimatter nuggets are strongly interacting but macroscopically large. They do not contradict any of the many known observational constraints on dark matter or antimatter for three main reasons [21]:

- They carry a huge (anti)baryon charge $|B| \gtrsim 10^{25}$, and so have an extremely tiny number density;
- The nuggets have nuclear densities, so their effective interaction is small $\sigma/M \sim 10^{-10}$ cm^2/g, well below the typical astrophysical and cosmological limits which are on the order of $\sigma/M < 1$ cm^2/g;
- They have a large binding energy $\sim \Delta$, such that baryon charge in the nuggets is not available to participate in big bang nucleosynthesis (BBN) at $T \approx 1$ MeV.

To reiterate: the weakness of the visible-dark matter interaction is achieved in this model due to the small geometrical parameter $\sigma/M \sim B^{-1/3}$ rather than due to a weak coupling of a new fundamental field with standard model particles. In other words, this small effective interaction $\sim \sigma/M \sim B^{-1/3}$ replaces a conventional requirement of sufficiently weak interactions of the visible matter with WIMPs.

As we already mentioned, this model when DM is represented by quark and antiquark nuggets is consistent with fundamental astrophysical constraints. Furthermore, there are a number of frequency bands where some excess of emission was observed, but not explained by conventional astrophysical sources. Our comment here is that this model may explain some portion, or even entire excess of the observed radiation in these frequency bands. This phenomenological part of the proposal is the key ingredient in our advocacy of the model, and may play very important role for interpretation of the present and future observations. Therefore, we devote next section 1.2 to review the original results [22–31] where predictions of the model have been confronted with the observations in specific frequency bands covering more than eleven orders of magnitude, from radio frequency with $\omega \sim 10^{-4}$ eV to γ rays with $\omega \sim 10$ MeV. We also mention in section 1.2 some interesting results [32–36] which are presently perfectly consistent with the model. However, in future, similar studies with modest improvements will provide a powerful test of the viability of the quark nugget dark matter model.

One should emphasize here that the corresponding analysis [22–31] is determined by conventional physics, and as such all effects are calculable from

the first principles. In other words, the model contains no tuneable fundamental parameters, except for a single mean baryon number of a nugget $\langle B \rangle \sim 10^{25}$ which enters all the computations [22–31] as a single normalization factor. At the same time, the crucial assumptions of the model, such as specific mechanisms on the baryon charge separation and dynamics of the nugget formation, etc, have never been explored in our previous studies.

We believe that the phenomenological success [22–31] of the model warrants further theoretical studies of this framework, in spite of its naively counter-intuitive nature. Therefore, the present work should be considered as the first step in this direction where we attempt to develop the theoretical framework to address (and hopefully answer) some of the hardest questions about a possible mechanism for the nuggets' formation during the QCD phase transition in strongly coupled regime when even the phase diagram at $\theta \neq 0$ as a function of the chemical potential μ and temperature T is still unknown, see footnote 2.

The structure of this work is as follows. In section 1.2 we briefly review the observational constraints on the model. In section 2.1 we highlight the basic assumptions and ingredients of this framework, while in sections 2.2 and 2.3 we present some analytical estimates which strongly substantiate the idea that such heavy objects indeed can be formed and survive until the present epoch during the QCD phase transition in early Universe. Section 2.4 as well as Appendices A and B are devoted to a number of technical details which support our basic claim.

In chapter 3 we argue that there will be the preferential formation of one species of nuggets over another. This preference is determined by the dynamics of the axion field $\theta(x)$ which itself is correlated on the scales of the Universe at the beginning of the nuggets' formation. Finally, in chapter 4 we comment on implications of our studies to direct axion search experiments.

To conclude this long introduction: the nuggets in our framework play a *dual* role: they serve as the DM candidates and they also explain the observed asymmetry between matter and antimatter. These two crucial elements of the proposal lead to very generic consequence of the entire framework expressed by eq. (1.1). This basic generic result is not very sensitive to any specific details of the model, but rather, entirely determined by two fundamental ingredients of the framework:
• the contribution to the present day density of both types of matter (visible and dark) are proportional to one and the same fundamental scale $\sim \Lambda_{\rm QCD}$;
• the preferential formation of one species of nuggets over another is correlated on huge cosmological scales where $\mathcal{CP}$ violating axion phase $\theta(x)$ remains coherent just a moment before the QCD phase transition.

The readers interested in the cosmological consequences, rather than in technical computational details may directly jump to section 2.1 where we formulate the basics ingredients of the proposal, to section 3.2 where we explain the main model-independent consequence (1.1) of this framework, and to chapter 4 where we make few comments on implications to other axion search experiments, including microwave cavity [9–11, 14] and the Orpheus experiments [15].

1.2 Quark (anti) nugget DM confronting the observations

While the observable consequences of this model are on average strongly suppressed by the low number density of the quark nuggets $\sim B^{-1/3}$ as explained above, the interaction of these objects with the visible matter of the galaxy will necessarily produce observable effects. Any such consequences will be largest where the densities of both visible and dark matter are largest such as in the core of the galaxy or the early universe. In other words, the nuggets behave as a conventional cold DM in the environment where density of the visible matter is small, while they become interacting and emitting radiation objects (i.e. effectively become visible matter) when they are placed in the environment with sufficiently large density.

The relevant phenomenological features of the resulting nuggets are determined by properties of the so-called electro-sphere as discussed in original refs. [22–31]. These properties are in principle, calculable from first principles using only the well established and known properties of QCD and QED. As such the model contains no tunable fundamental parameters, except for a single mean baryon number $\langle B \rangle$ which itself is determined by the axion mass m_a as we already mentioned.

A comparison between emissions with drastically different frequencies from the centre of galaxy is possible because the rate of annihilation events (between visible matter and antimatter DM nuggets) is proportional to the product of the local visible and DM distributions at the annihilation site. The observed fluxes for different emissions thus depend through one and the same line-of-sight integral

$$\Phi \sim R^2 \int d\Omega dl [n_{\rm visible}(l) \cdot n_{DM}(l)], \tag{1.6}$$

where $R \sim B^{1/3}$ is a typical size of the nugget which determines the effective cross section of interaction between DM and visible matter. As $n_{DM} \sim B^{-1}$

the effective interaction is strongly suppressed $\sim B^{-1/3}$ as we already mentioned in the Introduction. The parameter $\langle B\rangle \sim 10^{25}$ was fixed in this proposal by assuming that this mechanism saturates the observed 511 keV line from the galactic centre [22, 23], which resulted from annihilation of the electrons from visible matter and positrons from anti-nuggets. It has been also assumed that the observed dark matter density is saturated by the nuggets and anti-nuggets. Such assumptions would correspond to an average baryon charge $\langle B\rangle \sim 10^{25}$ for typical density distributions $n_{\rm visible}(r), n_{DM}(r)$ entering (1.6). Other emissions from different bands are expressed in terms of the same integral (1.6), and therefore, the relative intensities are completely determined by internal structure of the nuggets which is described by conventional nuclear physics and basic QED. We present a short overview of these results below.

Some galactic electrons are able to penetrate to a sufficiently close to the surface of the anti-nuggets. These events no longer produce the characteristic positronium decay spectrum (511 keV line with a typical width of order $\sim$ few keV accompanied by the conventional continuum due to 3γ decay) but a direct non-resonance $e^-e^+ \to 2\gamma$ emission spectrum. The transition between the resonance positronium decays and non-resonance regime is determined by conventional QED physics and allows us to compute the strength and spectrum of the MeV scale emissions relative to that of the 511 keV line [24, 25]. Observations by the Comptel satellite indeed show some excess above the galactic background consistent with our estimates.

Galactic protons incident on the anti-nugget will penetrate some distance into the quark matter before annihilating into hadronic jets. This process results in the emission of Bremsstrahlung photons at x-ray energies [26]. Observations by the Chandra observatory apparently indicate an excess in x-ray emissions from the galactic centre.

Hadronic jets produced deeper in the nugget or emitted in the downward direction will be completely absorbed. They eventually emit thermal photons with radio frequencies [27, 28]. Again the relative scales of these emissions may be estimated and is found to be in agreement with observations.

These apparent excess emission sources have been cited as possible support for a number of dark matter models as well as other exotic astrophysical phenomenon. At present however they remain open matters for investigation and, given the uncertainties in the galactic spectrum and the wide variety of proposed explanations are unlikely to provide clear evidence in the near future. Therefore, it would be highly desirable if some direct detection of such objects is found, similar to direct searches of the WIMPs.

While direct searches for WIMPs require large sensitivity, a search for very massive dark matter nuggets requires large area detectors. If the dark matter consists of quark nuggets, they will have a flux of

$$\frac{dN}{dA\ dt} = nv \approx \left(\frac{10^{25}}{B}\right) \mathrm{km}^{-2}\mathrm{yr}^{-1}. \tag{1.7}$$

Though this flux is far below the sensitivity of conventional dark matter searches it is similar to the flux of cosmic rays near the Greisen-Zatsepin-Kuzmin (GZK) limit. As such present and future experiments investigating ultrahigh energy cosmic rays may also serve as search platforms for dark matter of this type.

It has been suggested that large scale cosmic ray detectors may be capable of observing quark (anti-) nuggets passing through the earth's atmosphere either through the extensive air shower such an event would trigger [29] or through the geosynchrotron emission generated by the large number of secondary particles [30], see also [31] for review.

It has also been estimated in [32] that, based on Apollo data, nuggets of mass from $\sim$ 10 kg to 1 ton (corresponding to $B \sim 10^{28\text{-}30}$) must account for less than an order of magnitude of the local dark matter. While our preferred range of $B \sim 10^{25}$ is somewhat smaller and is not excluded by [32], we still believe that $B \geq 10^{28}$ is not completely excluded by the Apollo data, as the corresponding constraints are based on specific model dependent assumptions about the nugget mass-distribution.

It has also been suggested that the ANITA experiment may be sensitive to the radio band thermal emission generated by these objects as they pass through the antarctic ice [33]. These experiments may thus be capable of adding direct detection capability to the indirect evidence discussed above, see Fig.1.2 taken from [33] which reviews these constarints.

It has been also suggested recently [34] that the interactions of these (anti-) nuggets with normal matter in the Earth and Sun will lead to annihilation and an associated neutrino flux. Furthermore, it has been claimed [34] that the antiquark nuggets cannot account for more than 20% of the dark matter flux based on constraints for the neutrino flux in 20-50 MeV range where sensitivity of the underground neutrino detectors such as SuperK have their highest signal-to-noise ratio.

However, the claim [34] was based on assumption that the annihilation of visible baryons with antiquark nuggets generate the neutrino spectrum similar to conventional baryon- antibaryon annihilation spectrum when the large number of produced pions eventually decay to muons and consequently to highly energetic neutrinos in the 20-50 MeV energy range. Precisely these

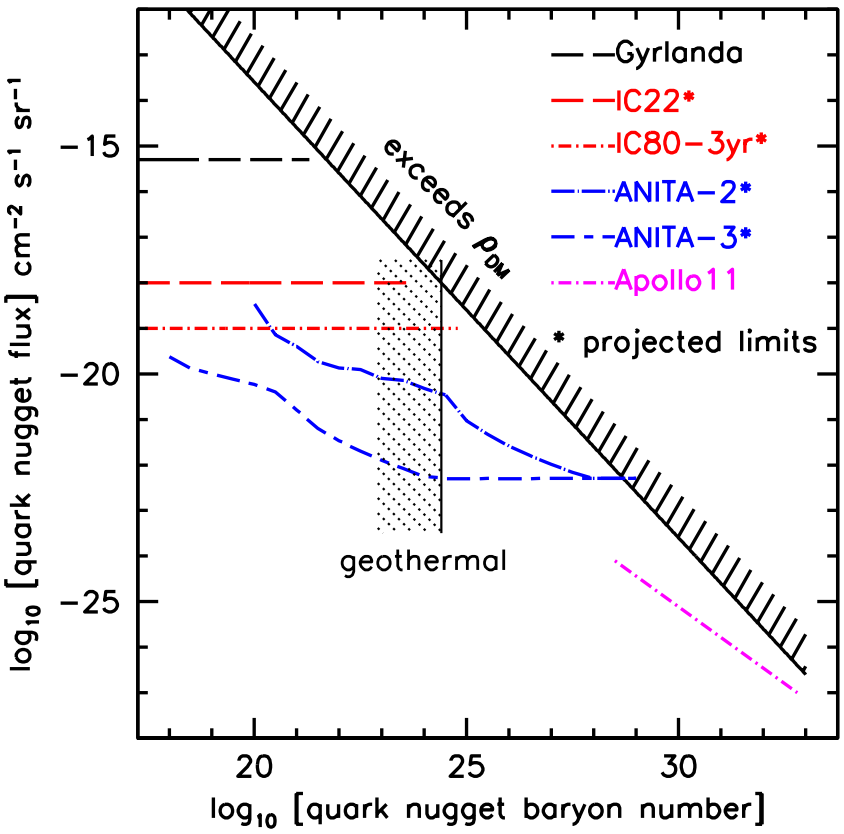

Figure 1.2: Limits on quark nugget mass and fluxes based on current (and future) constraints, taken from [33]. Our preferable value $\langle B \rangle \sim 10^{25}$ is translated to the axion mass $m_a \simeq 10^{-4}$ eV according to the scaling relation (1.3). The corresponding constraints expressed in terms of m_a have important implication for the direct axion search experiments as discussed in chapter 4. Orpheus experiment "B" is designed to be sensitive exactly to this value of the axion mass $m_a \simeq 10^{-4}$ eV, see Fig.4.1.

highly energetic neutrinos play the crucial role in analysis [34]. However, in most CS phases the lightest pseudo Goldstone mesons (the pions and Kaons) have masses in the 5-20 MeV range [17, 18] in huge contrast with hadronic confined phase where $m_\pi \sim 140$ MeV. Therefore, such light pseudo Goldstone mesons in CS phase cannot produce highly energetic neutrinos in the 20-50 MeV energy range and thus are not subject to the SuperK constraints [36].

We conclude this brief overview on observational constraints of the model with the following remark. This model which has a single fundamental parameter (the mean baryon number of a nugget $\langle B\rangle \sim 10^{25}$, corresponding to the axion mass $m_a \simeq 10^{-4}$ eV), and which enters all the computations is consistent with all known astrophysical, cosmological, satellite and ground based constraints as highlighted above. Furthermore, in a number of cases the predictions of the model are very close to the presently available limits, and very modest improving of those constraints may lead to a discovery of the nuggets. Even more than that: there are a number of frequency bands where some excess of emission was observed, and this model may explain some portion, or even entire excess of the observed radiation in these frequency bands.

In the light of this (quite optimistic) assessment of the observational constraints of this model it is quite obvious that further and deeper studies of this model are worthwhile to pursue. The relevant developments may include, but are not limited, to such hard problems as formation mechanisms during the QCD phase transition in early Universe, even though many key elements for proper addressing those questions at $\theta \neq 0, \mu \neq 0, T \neq 0$ are still largely unknown in strongly coupled QCD as shown on Fig.1.1. This work is the first step in the direction to explore a possible mechanism of formation of the nuggets.

Chapter 2

Formation of the Nuggets

As mentioned in the preceding chapter, the observational consequence of the nuggets have been studied for a long time. However, the formation aspect is previously just a conjecture. Taken as another motivation, this chapter (and this thesis) is dedicated to investigating the local formation of a nugget.

2.1 The crucial ingredients of the proposal

1. First important element of this proposal is the presence[5] of the topological objects, the axion domain walls [37]. As usual, it is assumed that the Peccei-Quinn symmetry[6] is broken after inflation. As we already mentioned the θ parameter is an angular variable, and therefore supports various types of domain walls, including the so-called $N_{DW} = 1$ domain walls when θ interpolates between one and the same physical vacuum state with the same energy $\theta \to \theta + 2\pi n$. The axion domain walls may form at the same moment when the axion potential get tilted, i.e. at the moment T_a when the axion field starts to roll due to the misalignment mechanism. The tilt becomes much more pronounced at the phase transition when the chiral condensate forms at T_c. In general one should expect that the $N_{DW} = 1$ domain walls form once the axion potential is sufficiently tilted to track (anti)quarks, i.e. anywhere between T_a and T_c. In the conventional models, T_a and T_c are usually considered as about 1 GeV and 170 MeV respectively.

Much later it has been realized that the axion (along with η') domain walls in general, demonstrate a sandwich-like substructure on the QCD scale $\Lambda_{QCD}^{-1} \simeq$ fm. The arguments supporting the QCD scale substructure inside

[5] To be specific, here mainly refers to the time after the QCD phase transition T_c when the domain walls are sufficiently tilted. Also see the the detailed explanation in this paragraph.

[6] Peccei-Quinn symmetry, is a proposed U(1) symmetry in order to resolve the puzzling strong CP problem. Such symmetry predicts the existence of axion, a neutral and ultralight psuedoscalar particle. Especially, axion may roll to a near potential minimum when the symmetry is spontaneously broken. This is also known as the misalignment mechanism.

the axion domain walls are based on analysis [38] of QCD in the large N limit with inclusion of the η' field[7] and independent analysis [39] of supersymmetric models where a similar θ vacuum structure occurs.

One should remark here that the described structure is a classically stable configuration. In particular, the η' field cannot decay to 2γ simply due to the kinematical reasons when a single η' field is off-shell (if not annihilated with another off-shell anti-field), and cannot be expressed as a superposition of on-shell free particles. It can only decay through the tunneling, and therefore, such $N_{DW} = 1$ domain walls are formally metastable rather than absolutely stable configurations.

2. Second important element is that in addition to these known QCD substructures [38–40] of the axion domain walls expressed in terms of the η' fields, there is another substructure (the baryonic fields, see below) with a similar QCD scale which carries the baryon charge. Precisely this novel feature of the domain walls which was not explored previously in the literature will play a key role in our proposal because exactly this new effect will be eventually responsible for the accretion of the baryon charge by the nuggets. Depending on the sign of the baryon charge, either quarks or anti-quarks are favoured to accrete on a given closed domain wall making eventually the quark nuggets or anti-nuggets. The sign is chosen randomly such that equal number of quark and antiquark nuggets are formed if the external environment is CP even, which is the case when fundamental $\theta = 0$. One can interpret this phenomenon as a *local spontaneous symmetry breaking effect*, when on the scales of order the correlation length of the axion field ξ the nuggets may acquire a positive or negative baryon charge with equal probability, as discussed in great details in next section 2.2.

3. Next important ingredient of the proposal is the Kibble-Zurek mechanism [8] which gives a generic picture of formation of the topological defects during a phase transition, see original papers [41], review [42] and the textbook [43]. In our context the Kibble-Zurek mechanism suggests that once the axion potential is sufficiently tilted the $N_{DW} = 1$ domain walls form. The potential becomes much more pronounced when the chiral condensate forms at T_c. After some time after T_a the system is dominated by a single,

[7] The η' field has the special property that it enters the effective Lagrangian in unique combination $[\theta - \eta'(x)]$ where the θ parameter in the present context plays the role of the axion dynamical field $\theta(x)$. A similar structure is known to occur in CS phase as well. The corresponding domain walls in CS phase have been also constructed [40].

[8] When topological objects, such as domain walls, kinks, and strings, form from spontaneous symmetry breaking. Kibble-Zurek mechanism describes their dynamical properties like correlation length, tension, and energy density.

percolated, highly folded and crumpled domain wall of very complicated topology of scale of the cosmic event horizon d_H. In addition, there will be a finite portion of the closed walls (bubbles) with typical size of order correlation length $\xi(T)$, which is defined [9] as an average distance between folded domain walls at temperature T. It is known that the probability of finding closed walls with very large size $R \gg \xi$ is exponentially small. Furthermore, numerical simulations suggest [43] that approximately 87% of the total wall area belong to the percolated large cluster, while the rest is represented by relatively small closed bubbles with sizes $R \sim \xi$.

The key point for our proposal is the existence of these finite closed bubbles made of the axion domain walls[10]. One should remark here that these closed bubbles had been formed sometime after T_a when original θ parameter has not settled yet to its minim value. It implies that the domain wall evolution starts at the time when θ parameter is not yet zero[11]. Normally it is assumed that these closed bubbles collapse as a result of the domain wall pressure, and do not play any significant role in dynamics of the system. However, as we already mentioned in Introduction the collapse of these closed bubbles is halted due to the Fermi pressure acting inside of the bubbles. Therefore, they may survive and serve as the dark matter candidates.

The percolated network of the domain walls will decay to the axions in conventional way as discussed in [44–46]. Those axions (along with the axions produced by the conventional misalignment mechanism [45, 47]) will contribute to the dark matter density today. The corresponding contribution to dark matter density is highly sensitive to the axion mass as $\Omega_{\rm dark} \sim m_a^{-1}$. Axion may saturate the observed dark matter density if $m_a \simeq 10^{-6}$ eV [9–16], while it may contribute very little to $\Omega_{\rm dark}$ if the axion mass is slightly

[9] The definition of ξ here refers to the average distance between any two domain walls, disregard closed or open. For axion field, $\xi \sim m_a^{-1}$ is generic from the Kibble-Zurek mechanism and therefore QCD insensitive.

[10] The presence of such closed bubbles in numerical simulations in context of the axion domain wall has been mentioned in [11], where it was argued that these bubbles would oscillate and emit the gravitational waves. However, we could not find any further details on the fate of these closed bubbles in the literature.

[11] This θ parameter in our work is defined as the value of θ at the moment when the domain walls form. It is not exactly the same value as the misalignment angle which normally enters all the computations due to the conventional misalignment mechanism [45, 47]. This is because the temperature when the domain walls form and the temperature T_a when the axion field starts to roll do not exactly coincide though both effects are due to the same axion tilted potential. The crucial point is that the θ parameter, as defined above, could be numerically small, nevertheless, it preserves its coherence over entire Universe, see chapter 3 for the details.

heavier than $m_a \simeq 10^{-6}$ eV. In contrast, in our framework an approximate relation $\Omega_{\rm dark} \approx \Omega_{\rm visible}$ holds irrespectively to the axion mass m_a.

We shall not elaborate on the production and spectral properties of these axions in the present work. Instead, the focus of the present thesis is the dynamics of the closed bubbles, which is normally ignored in computations of the axion production. Precisely these closed bubbles, according to this proposal, will eventually become the stable nuggets and may serve as the dark matter candidates.

As we already mentioned the nugget's contribution to $\Omega_{\rm dark}$ is not very sensitive to the axion mass, but rather, is determined by the formation temperature $T_{\rm form}$ as explained in Introduction, see also footnote 4 with few important comments on this. The time evolution of these nuggets after their formation is the subject of section 2.3.

4. The existence of CS phase in QCD represents the next crucial element of our scenario. The CS has been an active area of research for quite some time, see review papers [17, 18] on the subject. The CS phase is realized when quarks are squeezed to the density which is few times nuclear density. It has been known that this regime may be realized in nature in neutron stars interiors and in the violent events associated with collapse of massive stars or collisions of neutron stars, so it is important for astrophysics.

The force which squeezes quarks in neutron stars is gravity; the force which does an analogous job in early universe during the QCD phase transition is a violent collapse of a bubble of size $R \sim \xi(T)$ formed from the axion domain wall as described in item **3** above. If the number density of quarks trapped inside of the bubble (in the bulk) is sufficiently large, the collapse stops due to the internal Fermi pressure. In this case the system in the bulk may reach the equilibrium with the ground state being in a CS phase. As we advocate in section 2.3 this is very plausible fate of a relatively large size bubbles of size $R \sim \xi(T)$ made of the axion domain walls which were produced after the QCD phase transition.

5. If θ vanishes, then an equal number of nuggets and anti-nuggets would form. However, the $\mathcal{CP}$ violating θ parameter (the axion field), which is defined as value of θ at the moment of domain wall formation generically is not zero, though it might be numerically quite small. Precisely the dynamics of the coherent axion field $\theta(x)$ leads to preferences in formation of one species of nuggets, as discussed in chapter 3. This sign-preference is correlated on the scales where the axion field $\theta(x)$ is coherent, i.e. on the scale of the entire Universe at the moment of the domain wall formation. As we already mentioned, the generic consequence of this framework (1.1) is not very sensitive to an absolute value of θ at the moment of the domain

wall formation, see comment in footnote 4 on this matter. One can say that the coherent axion filed $\theta(x) \neq 0$, being numerically small, plays the role of the $\mathcal{CP}$ violating catalyst which determines a preferred direction for *separation of the baryon charges* on the Universe scale. This role of $\mathcal{CP}$ violation in our proposal is quite different from the role it plays in conventional "baryogenesis" mechanisms.

2.2 Accretion of the baryon charge

From now on and until chapter 3 we focus on the dynamics of a single closed bubble produced during the domain wall formation as described in item **3** in section 2.1. The correlation length $\xi(T)$ is defined as an average distance between folded domain walls at temperature T. We assume[12] that initial size of the bubble $\xi(T)$ is sufficiently large., few times larger than the axion domain wall width $\sim m_a^{-1}$, such that one can locally treat the surface of the closed bubble being flat.

The main goal of this section is to demonstrate that such a bubble will generically acquire a baryon (or antibaryon) charge in very much the same way as the η' field was dynamically accreted as originally discussed in [38] and briefly explained above as item **2** in section 2.1. In other words, we shall argue in this section that the bubbles with baryon or antibaryon charge will be copiously produced during the phase transition as they are very generic configurations of the system. In both cases the effect emerges as a result of the nontrivial boundary conditions formulated far away from the domain wall core when the field assumes physically the same but topologically distinct vacuum states on opposite sides of the axion domain wall.

The technique we shall adopt in this section has been previously used to study the generation of the galactic magnetic field in the domain wall background [48]. This method makes the approximation that the domain wall is flat and that translational and rotational symmetries are preserved in the plane of the wall (which we take to be the x–y plane). These approximations are marginally justified in our case because the initial curvature $R \sim \xi(T)$ is assumed to be few times larger that the width of the wall $\sim m_a^{-1}$.

Once this approximation is made, we can reformulate the problem in $1+1$ dimensions (z and t) and calculate the density of the bulk (of baryonic accumulation) properties along the domain wall. To regain the full four-dimensional bulk properties, we shall estimate the density of the particles

[12] This is a marginal assumption, but can be justified as in the later section 2.4.

in the x–y plane to obtain the appropriate density and degeneracy factors for the bulk density.

We proceed to demonstrate this technique by computing the accumulation of baryon charge along the wall. We take the standard form for the interaction between the pseudo-scalar fields and the fermions (quarks) which respect all relevant symmetries:

$$\mathcal{L}_4 = \bar{\Psi}\left(i\partial\!\!\!/ - me^{i[\theta(z)-\phi(z)]\gamma_5} - \mu\gamma_0\right)\Psi. \tag{2.1}$$

The subscript of "4" under the Lagrangian stands for dimensions, because it comes from the standard 4-dimensional Dirac equation after chiral rotation of $(\theta - \phi)$, where the anomaly term is neglected for the moment, but will be discussed in the next chapter 3. Here $\theta(z)$ and $\phi(z)$ are the dimensionless axion and η' domain wall solution. Parameter m is the the typical QCD scale of the problem, while μ is the typical chemical potential at a specific time in evolution of the system, see below with more precise explanations. We also simplify the problem by ignoring all flavour and colour indices, as well as an effective 4-fermi interactions, as our main goal is to explain the basic idea with simplified setting.

Parameter m in eq.(2.1) should not be literally identified with the quark mass, nor with the nucleon mass. Instead, this dimensional parameter $m \sim \Lambda_{QCD}$ should be thought as an effective coupling in our model when parameter m effectively describes the interaction with fermi field Ψ in all phases during the formation time, including the quark gluon plasma as well as hadronic and CS phases[13]. The same comment also applies to a numerical value of the chemical potential μ: it vanishes during initial time and becomes very large when CS phase sets in inside the nugget.

The strategy is to break (2.1) into two $1+1$ dimensional components by setting $\partial_x = \partial_y = 0$ (this is the approximation that the physics in the z direction decouples from the physics in the x–y plane) and then by manipulating the system of equations that result.

[13]In quark gluon phase the colour singlet η' field does not exist. However, the singlet phase which accompanied the quark field is still present in the system. The coefficient m in this phase can be computed using the instanton liquid model. At very high temperature the parameter m is proportional to the quark masses and indeed very small. When temperature decreases the instanton contribution grows very fast. At this point parameter m is proportional to the vacuum expectation value of the 't Hooft determinant. When temperature further decreases the parameter m is proportional to the diquark condensate in CS phase or the chiral condensate in the hadronic phase, see Fig.1.1. We shall not elaborate along this line by assuming $m \sim \Lambda_{QCD}$ for all our estimates which follow.

First, we introduce the following chiral components of the Dirac spinors[14]
:

$$\Psi_+ = \frac{1}{\sqrt{S}}\begin{pmatrix}\chi_1\\ \chi_2\end{pmatrix}, \qquad \Psi_- = \frac{1}{\sqrt{S}}\begin{pmatrix}\xi_1\\ \xi_2\end{pmatrix}, \tag{2.2}$$

$$\Psi = \frac{1}{\sqrt{2S}}\begin{pmatrix}\chi_1+\xi_1\\ \chi_2+\xi_2\\ \chi_1-\xi_1\\ \chi_2-\xi_2\end{pmatrix} = \frac{1}{\sqrt{2}}\begin{pmatrix}\Psi_+ + \Psi_-\\ \Psi_+ - \Psi_-\end{pmatrix}, \tag{2.3}$$

where S is the area of the wall. This normalization factor cancels the degeneracy factor proportional to S added in the text below.

The associated Dirac equation is

$$\begin{pmatrix}-me^{i(\phi-\theta)} & i(\partial_t+\partial_z)-\mu\\ i(\partial_t-\partial_z)-\mu & -me^{-i(\phi-\theta)}\end{pmatrix}\begin{pmatrix}\chi_1\\ \xi_1\end{pmatrix} = 0, \tag{2.4a}$$

$$\begin{pmatrix}-me^{i(\phi-\theta)} & i(\partial_t-\partial_z)-\mu\\ i(\partial_t+\partial_z)-\mu & -me^{-i(\phi-\theta)}\end{pmatrix}\begin{pmatrix}\chi_2\\ \xi_2\end{pmatrix} = 0. \tag{2.4b}$$

where we decouple the z coordinates from x and y by setting $\partial_x = \partial_y = 0$. Remember that we are looking for a two-dimensional Dirac equation, thus we want the kinetic terms to look the same. For this reason we should flip the rows and columns of the second equation. Doing this and defining the two two-dimensional spinors

$$\Psi_{(1)} = \begin{pmatrix}\chi_1\\ \xi_1\end{pmatrix}, \qquad \Psi_{(2)} = \begin{pmatrix}\xi_2\\ \chi_2\end{pmatrix}, \tag{2.5}$$

the equations have the following structure:

$$(i\hat{\gamma}^\nu\partial_\nu - me^{+i(\theta-\phi)\hat{\gamma}_5} - \mu\hat{\gamma_0})\Psi_{(1)} = 0 \tag{2.6a}$$

$$(i\hat{\gamma}^\nu\partial_\nu - me^{-i(\theta-\phi)\hat{\gamma}_5} - \mu\hat{\gamma_0})\Psi_{(2)} = 0 \tag{2.6b}$$

[14] We are using the standard representation here:

$$\gamma_0 = \begin{pmatrix}I & 0\\ 0 & -I\end{pmatrix}, \qquad \gamma_j = \begin{pmatrix}0 & \sigma_j\\ -\sigma_j & 0\end{pmatrix}, \qquad \gamma_5 = \begin{pmatrix}0 & I\\ I & 0\end{pmatrix},$$

$$\sigma_1 = \begin{pmatrix}0 & 1\\ 1 & 0\end{pmatrix}, \qquad \sigma_2 = \begin{pmatrix}0 & -i\\ i & 0\end{pmatrix}, \qquad \sigma_3 = \begin{pmatrix}1 & 0\\ 0 & -1\end{pmatrix}.$$

where the index $\nu \in \{t, z\}$, the Lorentz signature is $(1, -1)$ and we define the following two-dimensional version of the gamma matrices:

$$\hat{\gamma}_t = \sigma_1, \qquad \hat{\gamma}_z = -i\sigma_2, \qquad \hat{\gamma}_5 = \sigma_3.$$

These satisfy the proper two-dimensional relationships $\hat{\gamma}_5 = \hat{\gamma}_t\hat{\gamma}_z$ and $\hat{\gamma}_\mu\hat{\gamma}_\nu = g_{\mu\nu} + \epsilon_{\mu\nu}\hat{\gamma}_5$. We can reproduce equation (2.6) from the following effective two-dimensional Lagrangian density,

$$\begin{aligned}\mathcal{L}_2 =& \bar{\Psi}_{(1)}\left(i\hat{\gamma}^\mu\partial_\mu - me^{+i(\theta-\phi)\hat{\gamma}_5} - \mu\hat{\gamma_0}\right)\Psi_{(1)} + \\ &+\bar{\Psi}_{(2)}\left(i\hat{\gamma}^\mu\partial_\mu - me^{-i(\theta-\phi)\hat{\gamma}_5} - \mu\hat{\gamma_0}\right)\Psi_{(2)},\end{aligned} \tag{2.7}$$

where two different species of fermion with opposite chiral charge interact with the axion domain wall background determined by $\theta(z)$ and $\phi(z)$ fields. Note that, due to the normalization factor $1/\sqrt{S}$ we introduced above, the two-dimensional fields $\Psi_{(i)}$ have the correct canonical dimension 1/2.

We have thus successfully reduced our problem to a two-dimensional fermionic system. It is known that for systems that are constructed by components of (2.8) in $1 + 1$ dimensions, the fermionic representation is equivalent to a $1 + 1$ dimensional bosonic system through the following equivalences[49, 50]:

$$\bar{\Psi}_{(j)}i\hat{\gamma}^\mu\partial_\mu\Psi_{(j)} \to \frac{1}{2}(\partial_\mu\theta_j)^2, \tag{2.8a}$$

$$\bar{\Psi}_{(j)}\hat{\gamma}_\mu\Psi_{(j)} \to \frac{1}{\sqrt{\pi}}\epsilon_{\mu\nu}\partial^\nu\theta_j, \tag{2.8b}$$

$$\bar{\Psi}_{(j)}\Psi_{(j)} \to -m_0\cos(2\sqrt{\pi}\theta_j), \tag{2.8c}$$

$$\bar{\Psi}_{(j)}i\hat{\gamma}_5\Psi_{(j)} \to -m_0\sin(2\sqrt{\pi}\theta_j). \tag{2.8d}$$

The constant m_0 in the last two equations is a dimensional parameter of order $m_0 \sim m \sim \Lambda_{QCD}$. The exact coefficient of this factor depends on renormalization procedure and is only known for few exactly solvable systems but in all cases, is of order unity.

After making these replacements, we are left with the following two-dimensional bosonic effective Lagrangian density describing the two fields θ_1 and θ_2 in the domain wall background determined by $\phi(z)$ and $\theta(z)$:

$$\mathcal{L}_2 = \frac{1}{2}(\partial_\mu\theta_1)^2 + \frac{1}{2}(\partial_\mu\theta_2)^2 - U(\theta_1, \theta_2) + \frac{\mu}{\sqrt{\pi}}\frac{\partial(\theta_2 + \theta_1)}{\partial z} \tag{2.9}$$

where the effective potential is

$$\begin{aligned} U(\theta_1,\theta_2) = & - mm_0\left[\cos(2\sqrt{\pi}\theta_1-\phi+\theta)\right] \\ & - mm_0\left[\cos(2\sqrt{\pi}\theta_2+\phi-\theta)\right]. \end{aligned} \tag{2.10}$$

The conventional procedure to study the system (2.9) is to add the kinetic terms for the axion θ and the η' field ϕ into (2.9) and study a resulting solution depending on four dynamical fields by specifying all possible boundary conditions when the potential energy (2.10) assumes its minimal value[15]. In other words, one should take into account the dynamics of the θ and ϕ fields together with θ_1, θ_2 because the typical scales for ϕ, θ_1, θ_2 are roughly the same order of magnitude and of order of Λ_{QCD}. Recapitulate it: one cannot study the dynamics of θ_1, θ_2 field by neglecting their back reaction on the background axion and ϕ fields.

For our present purposes, however, we do not really need an explicit profile functions for the large number of different domain walls determined by various boundary conditions controlled by (2.10). The only important element relevant for our future discussions is the observation that some of the domain walls may carry the baryon (antibaryon) charge. Indeed, the domain walls which satisfy the boundary conditions

$$\begin{aligned} 2\sqrt{\pi}\theta_1(z=+\infty) - 2\sqrt{\pi}\theta_1(z=-\infty) = 2\pi n_1 \\ 2\sqrt{\pi}\theta_2(z=+\infty) - 2\sqrt{\pi}\theta_2(z=-\infty) = 2\pi n_2 \end{aligned} \tag{2.11}$$

carry the following baryon charge N defined for one particle Dirac equation

$$\begin{aligned} N &= \int d^3x \bar{\Psi}\gamma_0\Psi = \int dz \left(\bar{\Psi}_1\hat{\gamma_0}\Psi_1 + \bar{\Psi}_2\hat{\gamma_0}\Psi_2\right) \\ &= -\frac{1}{\sqrt{\pi}}\int_{-\infty}^{+\infty} dz \frac{\partial}{\partial z}(\theta_1+\theta_2) = -(n_1+n_2), \end{aligned} \tag{2.12}$$

where we express the final formula in terms of the auxiliary two-dimensional fields θ_1 and θ_2 and corresponding boundary conditions given by eq. (2.11). Factor S also cancels with our normalization for four dimensional Ψ field.

To complete the computations for four dimensional baryon charge B accumulated on the domain wall we need to multiply (2.12) by the degeneracy factor in vicinity of the domain wall which can be estimated as follows

$$B = N \cdot g \cdot \int \frac{d^2x_\perp d^2k_\perp}{(2\pi)^2} \frac{1}{\exp(\frac{\epsilon-\mu}{T})+1}, \tag{2.13}$$

[15] In fact it was precisely the procedure which has been adopted in [38] for a similar problem of computing of the profile functions of the axion, π- meson and η'-domain wall described by $\theta - \pi - \eta'$ fields.

where g is the appropriate degeneracy factor, e.g. $g \simeq N_c N_f$ in CS phase. We note that an additional degeneracy factor 2 due to the spin is already accounted for by parameter N defined in eq. (2.12). For high chemical potential $\mu \gg T$ corresponding to CS phase the baryon charge per unit area accreted in vicinity of the domain wall can be approximated as

$$\frac{B}{S} \simeq N \cdot \frac{g\mu^2}{4\pi}. \tag{2.14}$$

In the opposite limit of high temperature $\mu \ll T$ which corresponds to the quark gluon plasma phase, the corresponding magnitude can be estimated as follows

$$\frac{B}{S} \simeq N \cdot \frac{g\pi T^2}{24}. \tag{2.15}$$

It is instructive to compare the estimate (2.15) with number density $\mathcal{N}/V$ of all degrees of freedom in vicinity of the domain wall. Assuming that the baryon charge in the domain wall background is mainly concentrated on distances of order m^{-1} from the center of the domain wall we arrive to the following estimate for the ratio of the baryon number density bound to the wall in comparison with the total number density of all degrees of freedom responsible for the thermodynamical equilibrium in this phase

$$r \sim \frac{(B/S)\cdot m}{\mathcal{N}/V} \sim N\left(\frac{m}{T}\right)\left(\frac{\pi^3 g}{18\xi(3) g^*}\right), \tag{2.16}$$

where the effective degeneracy factor g^* for a quark gluon plasma is $g^* \simeq \left[\frac{3}{4}4N_cN_f + 2(N_c^2-1)\right]$ and $\xi(3) \simeq 1.2$ is the Riemann zeta function. Ratio (2.16) shows that the accreted quark density bounded to the domain wall at high temperature represents parametrically small contribution to all thermodynamical observables mainly because of a small parameter $m/T \ll 1$ in this phase. The situation drastically changes as we discuss in next section 2.3 when the temperature slowly decreases due to expansion of the Universe and the system enters the hadronic or CS phase, as shown on Fig. 1.1. At this point the baryon charge accumulation in the domain wall background becomes the major player of the system, which eventually leads to the formation of the CS nuggets or anti-nuggets when quarks (anti-quarks) fill entire volume of the nuggets (anti-nuggets).

We conclude this section with the following important comments. First, we argued that the domain walls in general accrete the baryon (or antibaryon) charge in vicinity of the centre of the domain wall. The effect in

many respects is similar to fractional charge localization on domain walls, while the rest of the charge is de-localized in the rest of volume of the system as discussed in original paper [51]. The effect is also very similar to previously discussed phenomenon on dynamical generation of the η' field in the domain wall background. The key point is that at sufficiently high temperature the $N_{DW} = 1$ domain walls form by the usual Kibble-Zurek mechanism as explained in section 2.1. The periodic fields $\theta, \phi, \theta_1, \theta_2$ may assume physically identical but topologically distinct vacuum values (2.12) on opposite sides of the walls. When the system cools down the corresponding fields inevitably form the domain wall structure, similar to analysis in hadronic [38] and CS phases [40].

We advocate the picture that the closed bubbles will be also inevitably formed as discussed in section 2.1. The collapse of these bubbles halts as a result of Fermi pressure due to the quarks accumulated inside the nugget during the evolution of the domain wall network. Next section 2.3 is devoted precisely the question on time evolution of these closed bubbles made of $N_{DW} = 1$ domain wall.

• The most important lesson of this section is that there is a variety of acceptable boundary conditions determined by potential (2.10) when the energy assumes its vacuum values. Some of the domain walls will cary zero baryon charge when the combination $(n_1 + n_2)$ vanishes according to (2.12). However, generically the domain walls will acquire the baryon or antibaryon charge. This is because the domain wall tension is mainly determined by the axion field while corrections due to QCD substructure will lead to a small correction of order $\sim m/f_a \ll 1$, similar to studies of the (axion -η'-π) domain wall [38]. Therefore, the presence of the QCD substructure with non vanishing $(n_1 + n_2) \neq 0$ increases the domain wall tension only slightly. In other words, accumulation of the baryon charge in vicinity of the wall does not lead to any suppression during the formation stage. Consequently, this implies that the domain closed bubbles carrying the baryon or antibaryon charge will be copiously produced during the phase transition as they are very *generic configurations of the system.* Furthermore, the baryon charge cannot leave the system during the evolution as it is strongly bound to the wall due to the topological reasons. The corresponding binding energy per quark is order of μ and increases with time as we discuss in the next section.

This phenomenon of "separation of the baryon charge" can be interpreted as a local version of spontaneous symmetry breaking of the baryon charge. This symmetry breaking occurs not in the entire volume in the ground state determined by the potential (2.10). Instead, the symmetry breaking occurs on scale $\xi(T)$ in vicinity of the field configurations which

describe the interpolation between physically identical but topologically distinct vacuum states (2.11). One should add that a similar phenomenon occurs with accumulation of the η' field in vicinity of the axion domain wall as described in [38]. However, one could not term that effect as a "local spontaneous violation" of the $U(1)_A$ symmetry because the $U(1)_A$ symmetry is explicitly broken by anomaly, in contrast with our present studies when the baryon charge is an exact symmetry of QCD. Nevertheless, the physics is the same in a sense that the closed bubble configurations generically acquire the axial as well as the baryon charge. This phenomenon as generic as formation of the topological domain walls themselves when the periodic fields ϕ, θ_1, θ_2 may randomly assume physically identical but topologically distinct vacuum values on the correlation lengths of order ξ.

Finally, one should also mention here that very similar effect of the "local $\mathcal{CP}$ violation" can be experimentally tested in heavy ion collisions in event by event basis where the so-called induced $\theta_{\rm ind}$- domain with a specific sign in each given event can be formed. This leads to the "charge separation effect" which can be experimentally observed in relativistic heavy ion collisions [52]. This "charge separation effect" in all respects is very similar to the phenomenon discussed in the present section. As an additional fact, the author's supervisor, Ariel Zhitnitsky, also involves in the studies [52] for a possibility to test the ideas advocated in this work by performing a specific analysis in the controllable "little Bang" heavy ion collision experiments, in contrast with "Big Bang" which happened billion of years ago. This field of research initiated in [52] became a hot topic in recent years as a result of many interesting theoretical and experimental advances, see recent review papers [53–55] on the subject.

2.3 Radius versus pressure in time evolution

We assume that a closed $N_{DW} = 1$ domain wall has been formed as discussed in previous section 2.1. Furthermore, we also assume that this domain wall is classified by non-vanishing baryon number $(n_1 + n_2)$ according to eq.(2.12). Our goal now is to study the time evolution of the obtained configuration. As we argue below the contraction of the bubbles halts as a result of the Fermi pressure due to baryon charge accreted during the evolution. As a result, the system comes to the equilibrium at some temperature $T_{\rm form}$ when the nuggets complete their formation. We want to see precisely how it happens, and what are the typical time scales relevant for these processes.

We start with the following effective Lagrangian describing the time

evolution of the closed spatially symmetric domain wall of radius $R(t)$,

$$\begin{aligned} L &= \frac{4\pi\sigma R^2(t)}{2}\dot{R}^2(t) - 4\pi\sigma R^2(t) \\ &+ \frac{4\pi R^3(t)}{3}\left[P_{\rm in}(\mu) - P_{\rm out}(t)\right] + [\text{other terms}]\,, \end{aligned} \tag{2.17}$$

where the "other terms" represents the effects that are not able to account in our simplified model, but are believed to be only minor corrections [16]. Here σ is the key dimensional parameter, the domain wall tension $\sigma \sim f_\pi m_\pi f_a \sim m_a^{-1}$ as reviewed in Introduction, see eq.(1.3). The tension σ, in principle, is also time-dependent parameter because the axion mass depends on time, but for qualitative analysis of this section we ignore this time dependence for now. We return to this question later in the text. Parameters $P_{\rm in}[\mu(t)]$ and $P_{\rm out}(t)$ represent the pressure inside and outside the bubble. The outside pressure in QGP phase at high temperature can be estimated as

$$\begin{aligned} P_{\rm out} &\simeq \frac{\pi^2 g^{\rm out}}{90} T_{\rm out}^4, \quad T_{\rm out} \simeq T_0 \left(\frac{t_0}{t}\right)^{1/2}, \\ g^{\rm out} &\simeq \left(\frac{7}{8} 4 N_c N_f + 2(N_c^2 - 1)\right) \end{aligned} \tag{2.18}$$

where $g^{\rm out}$ is the degeneracy factor, while $T_0 \simeq 100$ MeV and $t_0 \sim 10^{-4}$s represents initial temperature and time determined by the cosmological expansion. We also assume that the thermodynamical equilibrium is maintained at all times between inside and outside regions such that the temperature inside the bubble approximately follows the outside temperature $T_{\rm out}(t) \simeq T_{\rm in}(t)$. Very quick equilibration indeed is known to take place even in much faster processes such as heavy ion collisions. The fast equilibration in our case can be justified because the heat transport between the phases is mostly due to the light NG bosons which can easily penetrate the domain wall with little on no interaction, in contrast with quarks and baryons discussed in the previous section. This assumption will be justified a posteriori, see (2.47) on flux exchange rate between interior and exterior regions. Therefore, we believe our approximation $T_{\rm out}(t) \simeq T_{\rm in}(t)$ is sufficiently good, at least for qualitative estimates which is the main goal of this work.

The expression for the pressure inside the bubble $P_{\rm in}(t)$ depends on a number of quite nontrivial features of QCD such as the bag vacuum energy,

[16] Some neglected effects could be, for example, the realization of non-constancy of σ, which is nonetheless considered in the numerical computation, see Appendix B.

corrections due to the gap in CS phase and many other phenomena, to be discussed later in the text.

The equation of motion which follows from (2.17) is

$$\sigma\ddot{R}(t) = -\frac{2\sigma}{R(t)} - \frac{\sigma\dot{R}^2(t)}{R(t)} + \Delta P(\mu) - 4\eta\frac{\dot{R}(t)}{R(t)}, \tag{2.19}$$

where $\Delta P[\mu(t)] \equiv [P_{\rm in}(\mu) - P_{\rm out}(t)]$. We also inserted an additional term (which cannot be expressed in the Lagrangian formulation (2.17)), the shear viscosity η to the right hand side of the equation, which effectively describes the "friction" of the system when the domain wall bubble moves in "unfriendly" environment[17]. On the microscopical level this term effectively accounts for a large number of different effects which do occur during the time evolution. Such processes include, but are not limited to different scattering process by quarks, gluons or Nambu Goldstone Bosons in different phases. All these particles and quasiparticles interact between themselves and also with a moving domain wall. Furthermore, the annihilation processes which take place inside the bubble and which result in production of a large number of strongly interacting quasi-particles also contribute to η.

Having discussed an expression for $P_{\rm out}(T)$ and viscous term $\sim \eta$ we now wish to discuss the structure of the internal pressure $P_{\rm in}(\mu)$ which enters (2.19). It has a number of contributions which are originated from very different physics. We represent $P_{\rm in}(\mu)$ as as a combination of three terms to be discussed one by one in order,

$$P_{\rm in}(\mu) \simeq P_{\rm in}^{(\rm Fermi)}(\mu) + P_{\rm in}^{(\rm bag\ const)}(\mu) + P_{\rm in}^{(\rm others)}. \tag{2.20}$$

In this formula $P_{\rm in}^{(\rm Fermi)}$ can be represented as follows

$$P_{\rm in}^{(\rm Fermi)}(\mu) = \frac{E}{3V} = \frac{g^{\rm in}}{6\pi^2}\int_0^\infty \frac{k^3 dk}{\left[\exp(\frac{\epsilon(k)-\mu}{T}) + 1\right]}, \tag{2.21}$$

[17] We use conventional normalization factor of $4\eta\dot{R}(t)/R(t)$ for the viscous term. This normalization factor is the same which appears in the Rayleigh-Plesset equation in the classical hydrodynamics when the viscous term, the surface tension term $2\sigma/R(t)$ and the pressure term ΔP enter the equation in a specific combination as presented in (2.19). One should emphasize that our equation (2.19) describes the dynamics of the 2d surface characterized by the same surface tension σ in contrast with classical equation of the Rayleigh-Plesset equation describing a 3d spherical bubble in a liquid of infinite volume. This difference explains some distinctions between the kinetic terms proportional to factor $\sim \sigma$ in our case (2.19) in contrast with the classical Rayleigh-Plesset equation.

where we assume that quarks are massless and the chemical potential $\mu(t)$ implicitly depends on time as a result of the bubble's evolution (shrinking). The degeneracy factor in this formula is

$$g^{\rm in} \simeq 2N_cN_f, \tag{2.22}$$

where we keep only the quark contribution by neglecting the antiquarks. In other words, we simplify the problem by ignoring the time dependence of the degeneracy factor $g^{\rm in}(t)$ which effectively varies as a result of $\mu(t)$ variation.

Now we are in position to discuss $P_{\rm in}^{(\text{bag constant})}$ from (2.20) which can be represented as follows

$$P_{\rm in}^{(\text{bag const})}(\mu) \simeq -E_B \cdot \theta\left[\mu-\mu_1\right]\left[1-\frac{\mu_1^2}{\mu^2}\right], \tag{2.23}$$

where positive parameter $E_B \sim (150\ \text{MeV})^4$ is the famous "bag constant" from MIT bag model, see [4] for references and numerical estimates for this parameter in the given context of the nugget structure. The bag constant can be expressed in terms of the gluon and quark condensates in QCD. We shall not elaborate on this problem in the present work by referring to [4] with relevant studies in the given context.

The bag "constant" E_B describes the differences of vacuum energies (and therefore, vacuum pressure) in the interior and exterior regions of the nuggets. This difference occurs in our context because the phases realized outside and inside of the nugget are drastically distinct. For example, at the end of formation the outside region of the nugget is in cold hadronic phase, while inside region is in CS phase. The vacuum energies in these two phases are known to be drastically different. This term works as a "squeezer", similar to the role it plays in the MIT bag model, when the vacuum energy outside of the nugget is lower than the vacuum energy inside the nugget. Therefore it enters with the same sign minus as the domain wall pressure.

A specific μ- dependence used in (2.23) is an attempt to model a known feature of QCD that the absolute value of the vacuum energy decreases when the chemical potential increases. This feature is well established and tested in conventional nuclear matter physics, and it was analytically derived in simplified version of QCD with number of colours $N_c = 2$, see [4] for references and details. Our parametrization (2.23) corresponds to the behaviour when $P_{\rm in}^{(\text{bag constant})}(\mu) = 0$ for small chemical potentials $\mu \leq \mu_1$ when the vacuum energy inside and outside of the nuggets approximately equal. This term becomes very important "squeezer" at large chemical potential at $\mu \geq \mu_1$ when the system outside is in the hadronic vacuum state

while inside it is in a CS phase. The numerical value for parameter μ_1 can be estimated as $\mu_1 \sim 330$ MeV [4] when the baryon density is close to the nuclear matter density.

The last term entering (2.20) and coined as $P_{\rm in}^{(\rm others)}(\mu)$ is due to a large number of other effects which we ignore in present work. In particular, there is a conventional contribution due to the boson degrees of freedom which cancels the corresponding portion of $g^{\rm out}$ from (2.18) at high temperature, $T \gg \mu$. It does not play any important role in our analysis because we are mainly concerned with analysis of fermion degrees of freedom and building the chemical potential inside the bubble. Another effect which is worth to be mentioned is the formation of the gap in CS phase due to the quark pairing, similar to formation of the gap in conventional superconductors. The generation of the gap obviously decreases the energy of the system. There are many other phenomena which are known to occur in CS phase [17]. However, we expect that these effects are less important in comparison with the dominating contributions which are explicitly written down in equations (2.21) and (2.23).

The equation (2.19) can be numerically solved for $R(t)$ if time variation of the chemical potential $\mu(t)$ entering (2.21) and (2.23) is known. To study the corresponding time evolution for the chemical potential $\mu(t)$ we use expression (2.13) for the baryon charge bounded to the domain wall. We assume that the thermodynamical equilibrium is maintained between internal and external parts of the nugget such that $T_{\rm in}(t) \simeq T_{\rm out}(t)$. This assumption will be justified a posteriori, see discussions after eq.(2.47). At the same time the chemical potential is quickly increasing with time inside the nugget due to decreasing of the nugget's size. We also assume a fast equilibration for the chemical potential within the nugget in its entire volume. In other words, we describe the system using one and the same chemical potential in vicinity of the wall and deep inside the bubble. Justification for this assumption will be given later in the text.

With this picture in mind, we proceed by differentiating eq.(2.13) with respect to time to arrive to the following implicit equation relating $\mu(t)$ and $R(t)$ at fixed temperature T,

$$\dot{B} = \frac{Ng}{4\pi^2}\dot{S}(t)\int \frac{d^2k_\perp}{\left[\exp(\frac{\epsilon-\mu(t)}{T})+1\right]} \qquad (2.24)$$
$$+ \quad \frac{NgS}{4\pi^2}\frac{\dot{\mu}(t)}{T}\int \frac{d^2k_\perp \left[\exp(\frac{\epsilon-\mu(t)}{T})\right]}{\left[\exp(\frac{\epsilon-\mu(t)}{T})+1\right]^2} + (\text{fluxes}) = 0,$$

where term "fluxes" in (2.24) describes the loss of baryonic matter due to annihilation and other processes describing incoming and outgoing fluxes, to be discussed later in the text. The relation (2.24) gives an implicit relation between $\mu(t)$ and $R(t)$ which can be used for numerical studies of our equation (2.19) describing the time evolution of the system.

We shall discuss the physics related to incoming and outgoing fluxes in Appendix A. If we neglect this term which describes the loss of baryonic matter we can analytically solve (2.24) for small $\mu \ll T$ when one can use the Taylor expansion of the integrals entering (2.24). The result is

$$(\mu(t) - \mu_0) \simeq \frac{\pi^2 T}{6 \ln 2} \ln\left(\frac{R_0}{R(t)}\right), \tag{2.25}$$

where R_0 is initial size of the system at $t = t_0$ while $\mu_0 \simeq 0$ is initial chemical potential. One can explicitly see that the chemical potential builds in very fast when the nugget reduces its size only slightly. This formula (2.25) is only justified for very small $\mu(t)$. For larger values of μ one should use exact formula (2.24).

Finally, one should note that at the end of formation at time $t \to \infty$ when temperature $T \ll \mu$ the evolution stops, in which case all derivatives vanish, $\ddot{R}_{\rm form} = \dot{R}_{\rm form} = \dot{\mu}_{\rm form} = 0$. At this point the nugget assumes its final configuration with size $R \simeq R_{\rm form}$, and the equation (2.19) assumes the form

$$\frac{2\sigma}{R_{\rm form}} = P_{\rm in} = \frac{g^{\rm in}\mu^4}{24\pi^2} - E_B\left(1 - \frac{\mu_1^2}{\mu^2}\right), \quad \mu \geq \mu_1. \tag{2.26}$$

This condition is precisely the equilibrium condition studied in [4] with few neglected contributions (such as the quark-quark interaction leading to the gap). This is of course the expected result as the time evolution, which is the subject of the present work, must lead to the equilibrium configuration when the free energy assumes its minimum determined by (2.26).

One should recall that analysis of the equilibrium presented in ref. [4] with typical QCD parameters strongly suggests that the system indeed falls into CS phase when the axion domain wall pressure σ assumes its conventional value. At the same time, the equilibrium is not likely to emerge with the same typical QCD parameters without an additional external pressure related to the axion domain wall. In this sense the axion domain wall with extra pressure due to $\sigma \neq 0$ plays the role of an additional "squeezer" stabilizing the nuggets.

The key element of this section is equation (2.24) which is the direct consequence of a spontaneous accretion of the baryon (or antibaryon) charge

in the domain wall background as discussed in section 2.2. Precisely this equation explicitly shows that the chemical potential $\mu(t)$ grows very fast when the domain wall shrinks as a result of the domain wall pressure σ. The presence of a non-vanishing chemical potential in the vicinity of the domain wall obviously implies the generation of the binding forces between the fermions and the domain wall, such that a typical bound energy of a single fermion to the domain wall is of order of μ.

A generic solution of equations (2.19) and (2.24), as we discuss in the next section, shows an oscillatory behaviour of $R(t)$ with a slow damping of the amplitude such that the system eventually settles down at the equilibrium point (2.26). However, even the very first oscillation with initial $\mu_0 \approx 0$ leads to very fast growth of the chemical potential $\mu(t) \approx T$ as analytical estimates represented by eq.(2.25) shows. In the next section we develop a quantitative framework which allows us to analyze our basic equation (2.19) for $R(t)$ where time dependence $\mu(t)$ is implicitly expressed in terms of the same variable $R(t)$ as determined by (2.24).

2.4 Qualitative analysis

Our goal in this section is to solve for $R(t)$ and therefore $\mu(t)$ by solving (2.19) and (2.24), which implicitly relate both variables. We shall observe that a nugget experiences a large number of oscillations during its evolution with slow damping rate, and eventually settles down at the equilibrium point (2.26). This behaviour of the system will be coined as "underdamped oscillations". In next section 2.4.1 we formulate some assumptions and present the technical details, while the interpretation of the obtained results will be presented in section 2.4.2. We want to make a number of simplifications in our analysis in the present section to demonstrate the generic features of these oscillations. The numerical studies presented in Appendices A, B and C support our basic picture of oscillatory behaviour advocated in this section.

2.4.1 Assumptions, approximations, simplifications

Exact analytical analysis of either (2.19) or (2.24) can be obtained only during the first moment of the initial stage of evolution of the system when μ is sufficiently small (2.25). We need to understand the behaviour of the system for a much longer period of time. Thus, we make two important technical simplifications to proceed with our qualitative analysis. The first one is to neglect the term in (2.24) describing the fluxes. This assumption

will be supported by some estimates presented in Appendix A which show that incoming and outgoing fluxes cancel each other with very high accuracy, such that net flux is indeed quite small. Hence, (2.24) is now simplified to:

$$\dot{B} = \frac{d}{dt}\left\{ \frac{Ng}{4\pi^2} S \int \frac{d^2k_\perp}{\exp(\frac{\epsilon-\mu}{T})+1} \right\} = 0 \tag{2.27}$$

which means in this approximation, the baryonic charge is roughly conserved in the domain wall background at all times during the evolution of the system.

As our second simplification we neglect the mass of the fermions in comparison with temperature T and the chemical potential μ, i.e. we use the following dispersion relation $\epsilon = \sqrt{k_\perp^2 + m^2} \simeq k_\perp$ in vicinity of the domain wall. This approximation is somewhat justified in QGP and CS phases, and therefore along the path 3 as shown on Fig. 1.1. It is not literally justified for paths 1 and 2 as in the hadronic phase where the quark mass m should be identified with the so-called "constituent" quark mass which is proportional to the chiral condensate. Nevertheless, to simplify the problem we neglect the mass $m(T)$ for all paths in our qualitative analysis of the time evolution as we do not expect any drastic changes in our final outcome as a result of this technical simplification. With these assumptions we can approximate the integral entering eq. (2.27) as follows,

$$\int_0^\infty \frac{dk_\perp \cdot k_\perp}{e^{\frac{\epsilon(k_\perp)-\mu}{T}}+1} = T^2 \cdot I(\frac{\mu}{T}) \tag{2.28}$$
$$I(\frac{\mu}{T}) \simeq \frac{\pi^2}{6} + \frac{1}{2}\left(\frac{\mu}{T}\right)^2 - \frac{\pi^2}{12} e^{-\mu/T} + \mathcal{O}(\frac{\mu}{T} e^{-\mu/T})$$

where the omitted terms $\sim \frac{\mu}{T} e^{-\mu/T}$ will be neglected thereafter, as they will never dominate in neither small nor large limit of μ. One can numerically check that approximation (2.28) describes the relevant integral $I(\frac{\mu}{T})$ sufficiently well in the entire parametrical space of μ/T, see Appendix C with corresponding analysis. As a quick test of this approximation one can check that approximate expression (2.28) reproduces an exact (in the small μ limit) expression (2.25) with accuracy of order 15%, which is more than sufficient for our qualitative studies of this section.

As mentioned above, if flux term (2.24) is neglected, the curly-bracket term in (2.27) is a conserved quantity. Equating it to its initial values where $S(t=0) = 4\pi R_0^2$, $\mu(t=0) = \mu_0 \simeq 0$ one arrives to

$$T^2 R^2 \left[\frac{\pi^2}{6} + \frac{1}{2}\left(\frac{\mu}{T}\right)^2 - \frac{\pi^2}{12} e^{-\mu/T} \right] = \frac{\pi^2}{12} T_0^2 R_0^2. \tag{2.29}$$

In what follows we assume that the thermodynamical equilibration is established very quickly such that one can approximate $T \simeq T_0$ during the time evolution as we already discussed in the previous section 2.3. To simplify further the system we wish to represent the equation relating R and μ/T in the following form

$$f(R) \equiv \frac{\pi^2}{6}\left[\frac{1}{2}\left(\frac{R_0}{R}\right)^2 - 1\right] = \frac{1}{2}\left(\frac{\mu}{T}\right)^2 - \frac{\pi^2}{12}e^{-\mu/T}, \tag{2.30}$$

where we introduced function $f(R)$ for convenience of the analysis which follows. Essentially, the idea here is to simplify the basic equation (2.19) as much as possible to express the $\mu(t)-$ dependent terms entering through the pressure (2.20) in terms of $R(t)$ such that the equation (2.19) would assume a conventional differential equation form for a single variable $R(t)$.

Our next step is to simplify the expression for the Fermi pressure (2.21) entering (2.20) using the same procedure we used to approximate formula (2.28), i.e.

$$\begin{aligned} P_{\rm in}^{(\rm Fermi)} &= \frac{g^{\rm in}}{6\pi^2}\int_0^\infty \frac{k^3 dk}{\exp\left(\frac{\epsilon(k)-\mu}{T}\right)+1} \\ &\simeq \frac{g^{\rm in}T^4}{6\pi^2}\left\{\frac{7\pi^4}{60} + \frac{\pi^2}{2}\left(\frac{\mu}{T}\right)^2 - \frac{7\pi^4}{120}e^{-\mu/T} + \frac{1}{4}\left(\frac{\mu}{T}\right)^4 \right. \\ &\qquad \left. + \mathcal{O}(\frac{\mu}{T}e^{-\mu/T})\right\} \\ &\simeq \frac{g^{\rm in}T^4}{6}\left\{\frac{7\pi^2}{60} + \left[\frac{1}{2}\left(\frac{\mu}{T}\right)^2 - \frac{\pi^2}{12}e^{-\mu/T}\right] + \frac{1}{4\pi^2}\left(\frac{\mu}{T}\right)^4\right\} \\ &+ \frac{g^{\rm in}T^4}{6}\left\{\frac{\pi^2}{40}e^{-\mu/T} + \mathcal{O}(\frac{\mu}{T}e^{-\mu/T})\right\}. \end{aligned} \tag{2.31}$$

In what follows we neglect the last line in eq. (2.31). The justification for this procedure is the same as before: it produces a small contribution in entire region of μ in comparison with accounted terms. The technical advantage for this procedure is the possibility to rewrite (2.31) in terms of function of $R(t)$, rather than $\mu(t)$ using our relation (2.30).

The formula in the square bracket in (2.31) is just $f(R)$ defined by (2.30). The remaining $\left(\frac{\mu}{T}\right)^4$ term can be also expressed in terms of R by taking

square of (2.30):

$$\begin{aligned} f^2(R) &= \left[\frac{1}{2}\left(\frac{\mu}{T}\right)^2 - \frac{\pi^2}{12}e^{-\mu/T}\right]^2 \\ &\simeq \frac{1}{4}\left(\frac{\mu}{T}\right)^4 + \left(\frac{\pi^2}{12}\right)^2 + \mathcal{O}\left(\frac{\mu}{T}e^{-\mu/T}\right) \end{aligned} \tag{2.32}$$

where the correction term $\sim \mathcal{O}(\mu e^{-\mu/T})$ will be dropped in what follows, as before. Thus, we approximate $P_{\rm in}^{(\rm Fermi)}$ in terms of $R(t)$ as follows

$$P_{\rm in}^{(\rm Fermi)} \simeq \frac{g^{\rm in}T^4}{6}\left[\frac{7\pi^2}{60} + f(R) + \frac{f^2(R)}{\pi^2} - \frac{\pi^2}{144}\right]. \tag{2.33}$$

The expression for the Fermi pressure $P_{\rm in}^{(\rm Fermi)}(R)$ now is expressed in terms of R rather than in terms of μ as in the original expression (2.21).

We wish to simplify the expression for $P_{\rm in}^{(\rm bag\ const)}(\mu)$ entering (2.20) in a similar manner to express $P_{\rm in}^{(\rm bag\ const)}$ in terms of R. This contribution becomes important as discussed after eq. (2.23) only for sufficiently large μ. In this region $f(R)$ can be well approximated as

$$f(R) \simeq \frac{1}{2}\left(\frac{\mu}{T}\right)^2, \quad \mu \gg T \tag{2.34}$$

so that we have

$$P_{\rm in}^{\rm bag} \simeq -E_B \cdot \theta\left(\sqrt{2f(R)} - \frac{\mu_1}{T}\right)\left(1 - \frac{\mu_1^2}{2T^2 f(R)}\right). \tag{2.35}$$

As a result of these simplifications and approximations the pressure term which enters the basic equation (2.19), $\Delta P(\mu) \equiv [P_{\rm in}(\mu) - P_{\rm out}(t)]$ which was initially formulated in terms of the chemical potential μ inside the bubble can be now written entirely in terms of a single variable, the size of the bubble $R(t)$:

$$\begin{aligned} \Delta P[f(R)] \simeq{}& \frac{g^{\rm in}\pi^2}{6}T^4\left[\frac{79}{720} - \frac{g^{\rm out}}{15g^{\rm in}} + \frac{f(R)}{\pi^2} + \frac{f^2(R)}{\pi^4}\right] \\ & -E_B \cdot \theta\left(\sqrt{2f(R)} - \frac{\mu_1}{T}\right)\left(1 - \frac{\mu_1^2}{2T^2 f(R)}\right), \end{aligned} \tag{2.36}$$

where $f(R)$ is defined by eq. (2.30). With these technical simplifications the basic equation (2.19) can now be written as a second order differential equation entirely in terms of $R(t)$ rather than μ:

$$\sigma\ddot{R}(t) = -\frac{2\sigma}{R} - \frac{\sigma\dot{R}^2}{R} + \Delta P[f(R)] - 4\eta\frac{\dot{R}}{R}, \tag{2.37}$$

with $\Delta P[f(R)]$ determined by eq. (2.36).

This equation can be solved numerically. In fact, it is precisely the subject of Appendix B. However, the most important quantitative features of the obtained solution can be understood without any numerical studies, but rather using a simplified analytical analysis, which is precisely the subject of the next section.

2.4.2 Time evolution

As we already mentioned a nugget assumes its final form at $t \to \infty$ when all time derivatives vanish and the equation for the equilibrium is given by (2.26) at $T = 0$. In this section we generalize this equation for the equilibrium by defining $R_{\rm form}(T)$ as the solution of eq.(2.38), see below, at $T \neq 0$. In other words, the starting point of the present analysis at $T \neq 0$ is the equilibrium condition when the "potential" energy assumes its minimal value. The corresponding minimum condition is determined by equation

$$\frac{2\sigma}{R_{\rm form}} = \Delta P(R_{\rm form}), \tag{2.38}$$

where $\Delta P(R_{\rm form})$ is defined by eq.(2.36). This condition obviously reduces to eq. (2.26) at $t \to \infty$ when $\mu \gg T$.

We follow the conventional technique and expand (2.37) around the equilibrium value $R_{\rm form}(T)$ to arrive to an equation for a simple damping oscillator:

$$\frac{d^2(\delta R)}{dt^2} + \frac{2}{\tau}\frac{d(\delta R)}{dt} + \omega^2(\delta R) = 0, \tag{2.39}$$

where $\delta R \equiv [R(t) - R_{\rm form}]$ describes the deviation from the equilibrium position, while new parameters τ and ω describe the effective damping coefficient and frequency of the oscillations. Both new coefficients are expressed in terms of the original parameters entering (2.37) and are given by

$$\tau = \frac{\sigma}{2\eta} R_{\rm form} \tag{2.40a}$$

$$\omega^2 = -\frac{1}{\sigma}\frac{d\Delta P(R)}{dR}\bigg|_{R_{\rm form}} - \frac{2}{R_{\rm form}^2}. \tag{2.40b}$$

The expansion (2.39) is justified, of course, only for small oscillations about the minimum determined by eq.(2.38), while the oscillations determined by original equation (2.37) are obviously not small. However, our simple analytical treatment (2.39) is quite instructive and gives a good qualitative

understanding of the system. Our numerical studies presented in Appendix B fully support the qualitative picture presented below.

We start our qualitative analysis with estimates of the parameter ω which depends on $\frac{d\Delta P(R)}{dR}$ computed at $R = R_{\rm form}$ according to (2.40b). First of all, in this qualitative analysis we neglect the bag constant term $P_{\rm in}^{(\text{bag constant})}$ because it only starts to play a role for sufficiently large $\mu \geq \mu_1 \sim 330$ MeV, when formation is almost completed. This term obviously cannot change the qualitative behaviour of the system discussed below. Our numerical studies presented in Appendix B (where the bag constant term $\sim E_B$ is included in the analysis) support this claim.

The key element for our simplified analysis is the observation that the ratio $(R_0/R_{\rm form})^2 \geq 14$ is expected to be numerically large number. This expectation will be soon confirmed a posteriori. This observation considerably simplifies our qualitative analysis because in this case $\Delta P(R_{\rm form})$ defined by (2.36) can be approximated by a single term $\sim f^2(R)$ in square brackets in (2.36) as this term essentially saturates $\Delta P(R_{\rm form})$. This is because the function $f(R)/\pi^2$ becomes numerically large in the relevant region $f(R)/\pi^2 \sim (R_0/R_{\rm form})^2$ according to (2.30).

With these simplifications we can now estimate ω^2 as follows

$$\omega^2 \approx \left(\frac{g^{\rm in}\pi^2}{216}\right) \cdot \left(\frac{T^4}{\sigma R_{\rm form}}\right) \cdot \left(\frac{R_0}{R_{\rm form}}\right)^4 - \left(\frac{2}{R_{\rm form}^2}\right). \tag{2.41}$$

To simplify analysis further one can represent the last term as

$$\left(\frac{2}{R_{\rm form}^2}\right) = \left(\frac{1}{R_{\rm form}}\right) \cdot \left(\frac{\Delta P(R_{\rm form})}{\sigma}\right), \tag{2.42}$$

and keep the leading term $\sim f^2(R)$ in expression for $\Delta P(R_{\rm form})$. One can easily convince yourself that $\omega^2 > 0$ is always positive in this approximation such that the condition for a desired underdamped oscillations assumes a simple form

$$\frac{f(R_{\rm form})}{\pi^2} \gtrsim 1 \quad \Rightarrow \quad \left(\frac{R_0}{R_{\rm form}}\right) \gtrsim \sqrt{14} \tag{2.43}$$

when $\Delta P(R_{\rm form})$ defined by (2.36) is dominated by a single term $\sim (\frac{f}{\pi^2})^2$, which itself can be approximated by the leading quadratic term $\sim \left(\frac{R_0}{R}\right)^2$ according to (2.30). Our numerical studies presented in Appendix B support the numerical estimate (2.43).

One can also check that if condition (2.43) is not satisfied than system shows an "over-damped" behaviour when very few oscillations occur before complete collapse of the system, in which case the nuggets obviously do not form. These short-lived bubbles will never get to a stage when the temperature drops below the critical value T_{CS}. Therefore, a CS phase cannot form in these "short-lived" bubbles. It should be contrasted with "long-lived" bubbles with much longer formation-time of order τ, see comments below.

The condition (2.43) is extremely important for our analysis. It essentially states that the initial size of a closed bubble R_0 must be sufficiently large for a successful formation of a nugget of size $R_{\rm form}$. On the other hand, a formation of very large closed bubbles is strongly suppressed $\sim \exp[-(R_0/\xi)^2]$ by the KZ mechanism as reviewed in section 2.1. This constraint will be important in our estimation of a suppression factor in section 3.3 due to necessity to form a sufficiently large bubble (2.43) during the initial stage of formation.

Assuming that condition (2.43) is satisfied we estimate a typical oscillation frequency as follows

$$\omega \sim \frac{1}{R_{\rm form}} \sim m_a, \qquad t_{\rm osc} \simeq \omega^{-1} \simeq m_a^{-1} \tag{2.44}$$

where we used the scaling properties (1.3) to relate the nugget's size $R_{\rm form}$ with the axion mass m_a. One should emphasize that the estimate (2.44) is not sensitive to any approximations and simplifications we have made in our qualitative treatment of the time evolution in this section. In fact, all parameters entering relation (2.44) are expressible in terms of the QCD scale $\Lambda_{\rm QCD}$ and a single "external" parameter, the axion mass m_a, which we keep unspecified at this point. Of course we always assume that the axion mass may take any value from the observationally allowed window $10^{-6}{\rm eV} \lesssim m_a \lesssim 10^{-3}{\rm eV}$.

We now turn our attention to the damping coefficient defined in terms of the original parameters by eq. (2.40a). It is convenient to estimate the dimensionless combination $\omega\tau$ as follows

$$\omega\tau \simeq \frac{1}{R_{\rm form}} \cdot \left(\frac{\sigma}{2\eta} R_{\rm form}\right) \simeq \frac{\sigma}{2\eta} \sim \frac{m_\pi}{m_a} \sim 10^{11}, \tag{2.45}$$

where we substituted $\omega \sim R_{\rm form}^{-1}$ according to (2.44) and assumed that $\eta \sim m_\pi^3$ has conventional QCD scale of order ${\rm fm}^{-3}$ while the wall tension σ can be approximated with high accuracy as $\sigma \simeq m_\pi^4/m_a$. This relation implies that the damping is extremely slow on the QCD scales. Therefore, the

solution describing the time evolution of a "long-lived" bubble can be well approximated as follows

$$R(t) = R_{\rm form} + (R_0 - R_{\rm form})e^{-t/\tau}\cos\omega t \tag{2.46}$$

which is obviously a solution of the approximate equation (2.39). This solution represents an "under-damped" oscillating $R(t)$ with frequency $\omega \sim \frac{1}{R_{\rm form}}$ and damping time $\tau \sim \frac{\sigma}{2\eta}R_{\rm form}$. Precisely these "long-lived" bubbles will eventually form the DM nuggets.

The time scale (2.45) is very suggestive and implies that the damping term starts to play a role on very large scales when the cosmological expansion of the Universe with the typical scale $t_0 \simeq 10^{-4}s$ must be taken into account. We have not included the corresponding temperature variation in our studies because on the QCD scales (which is the subject of the present studies) the corresponding variations are negligible. However, the estimate (2.45) shows that for a proper analysis of the time scales τ the expansion of the Universe (and related to the expansion the temperature variation) must be included. The corresponding studies are beyond the scope of the present work. However, the important comment we would like to make here is that the emergent large time scale (2.45) is fully consistent with our anticipation that the temperature of the Universe drops approximately by a factor of ~ 3 or so when a CS phase forms in interior of the nugget during the formation period. It is quite obvious that if the time scale (2.45) were considerably shorter than the cosmological time scale $t_0 \simeq 10^{-4}s$ than the temperature $T \sim t^{-1/2}$ inside the nugget could not drop sufficiently deep into the region where CS sets in as plotted on Fig.1.1. Fortunately, the timescale (2.45) is long enough and automatically satisfies this requirement.

Now we want to elaborate on one more element of the dynamics which is also important for a successful formation of the nuggets. To be more specific, we want to discuss the flux of particle exchange, which was ignored in our qualitative analysis in this section and which is estimated in Appendix A. This flux describes the rate of number of particle flowing between inside and outside the system, which can be appreciably large even if the net baryonic flux is negligibly small. To be more precise, there are two kinds of fluxes, both investigated in Appendix A, that we are discussing in this thesis: the net flux of baryonic charge $\Delta\Phi \equiv \Phi_{\Rightarrow} - \Phi_{\Leftarrow}$, and the average flux of particle number $\langle\Phi\rangle \equiv \frac{1}{2}(\Phi_{\Rightarrow} + \Phi_{\Leftarrow})$. The first one corresponds to the flux term entering eq. (2.24); while the latter is important in understanding what is the typical time scale for a complete "refill" of the particles during the time evolution. The last question is important for understanding of the time scale for thermal equilibration.

We start our analysis with discussions of an average flux $\langle\Phi\rangle$ at small chemical potential. It is estimated to be $\langle\Phi\rangle \simeq 1$ fm^{-3} according to Appendix A. The magnitude of this flux can be fully appreciated by computing the total number of particle exchange per one cycle of the oscillation

$$\frac{2\pi}{\omega}\cdot 4\pi R^2_{\rm form}\cdot\langle\Phi\rangle \sim R^3_{\rm form}{\rm fm}^{-3} \sim |{\rm B}|\,, \tag{2.47}$$

where ω is a typical frequency oscillation estimated in (2.44) while $|B|$ is the total number of particles (quarks and antiquark) stored in the nugget. The physical meaning of this estimate is that a nugget can in principle entirely refill its interior with "fresh" particles within a few cycles of exchange. Similar estimate for the net baryon flux which includes $\Delta\Phi$ is suppressed, see Appendix A.

The main reason for emergence of this large scale in expression (2.47) is a long time scale of a single cycle (2.44) which is determined by the axion mass m_a rather than by QCD physics. Nevertheless, estimate (2.47) is quite remarkable and shows that even very low rate of chemical potential accretion of (anti)quarks being tracked per oscillation, the high exchange rate (2.47) is still sufficient enough to turn a baryonically neutral nugget into one completely filled with (anti)quarks. When the quarks become effectively massive as it happens in hadronic and CS phases, the flux for the exchange of the baryon charge is drastically decreased by a factor $\sim \exp(-m/T)$.

The same estimate (2.47) essentially holds for exchange of almost massless Nambu-Goldstone bosons for sufficiently high temperature. In fact, the lightest degrees of freedom play the crucial role in cooling processes of the interior of the nugget as these particles can easily penetrate the sharp domain wall structure. Therefore, the high exchange rate between exterior and interior of a nugget essentially implies that the thermal equilibrium is maintained in our system with very high precision due to a huge rate per cycle (2.47) when large number of degrees of freedom $\sim B$ have a chance of order one to interact with "fresh" particles from the exterior during a single cycle. Therefore, our assumption on thermal equilibrium between interior and exterior is justified a posteriori.

We conclude this section with few important comments. The most important result of this section is that the nuggets can be formed during the QCD phase transition provided the initial size of the nuggets is sufficiently large as stated in eq.(2.43), in which case they survive the evolution. The key role in this successful formation plays, of course, the effect of "local spontaneous violation" of the baryon symmetry as discussed in section 2.2 and explicitly expressed by eqs.(2.11) and (2.12). One should emphasize

that our qualitative analyses in this section are fully supported by numerical studies presented in Appendices A and B. Therefore, we do not expect that any numerical simplifications in our analysis may drastically change the basic qualitative results presented in this section.

Another important point is the observation (2.44) that a typical time scale for the oscillations is of order $t_{\rm osc} \simeq \omega^{-1} \simeq m_a^{-1}$. Both these estimates will be crucial elements in our analysis presented in next chapter 3: equation (2.43) will be important in estimate for efficiency of a bubble formation with a large size $\sim R_0$, while equation (2.44) will play a key role in our arguments suggesting a coherent preferential formation of one type of nuggets (baryonic or antibaryonic) on largest possible scale of the visible Universe.

Chapter 3

Baryon Charge Separation. Correlation on Cosmological Scales.

Until this section we mostly concentrated on the time evolution of a single nugget (or anti-nugget). The main lesson of our previous discussions is that such nuggets can be formed, remain stable configurations, and therefore, can serve as the dark matter candidates. In other words, the focus of our previous studies was a problem of a local separation of charges on small scales of order nugget's size. The key element of that separation of charges is eq. (2.11) which can be thought as a local version of spontaneous symmetry breaking of the baryon charge as explained in section 2.2. However, on a larger scale it is quite obvious that equal number of nuggets and anti-nuggets will be formed as a result of an exact symmetry as we discuss below.

This symmetry, however, does not hold anymore on large scales if the axion $\mathcal{CP}$ -odd coupling is included into consideration, which eventually leads to very generic, essentially insensitive to most parameters, consequence of this framework represented by eq.(1.1), which is the subject of next subsections 3.1 , 3.2. The subsection 3.3 is devoted to some more specific and model-dependent consequences of this framework. In particular, we want to estimate a suppression factor related to the necessary to form a large size bubble (2.43) in KZ mechanism.

3.1 Coherent axion field as the source of $\mathcal{CP}$ violation

First of all, let us show that the baryon charge hidden in nuggets on average is equal to the baryon charge hidden in anti-nuggets, of course with sign minus. Indeed, the analysis of the anti-nuggets can be achieved by flipping the sign of the chemical potential in eq. (2.9), i.e. $\mu \to -\mu$. One can restore the original form of the μ term in Lagrangian (2.9) by replacing

$\theta_1 \to -\theta_1$ and $\theta_2 \to -\theta_2$. Finally, one should change the signs for the axion θ and the pseudo-scalar singlet η' meson represented by ϕ field in the interaction term (2.10) to restore the original form of the Lagrangian. These symmetry arguments imply that as long as the pseudo-scalar axion field fluctuates around zero as conventional pseudo-scalar fields (as π, η' mesons, for example), the theory remains invariant under $\mathcal{P}$ and $\mathcal{CP}$ symmetries. Without this symmetry the number density and size distribution of the nuggets and anti-nuggets could be drastically different[18].

Therefore, the symmetry arguments suggest that on average an equal number of nuggets and anti-nuggets would form if the axion field is represented by a conventional quantum fluctuating field oscillating around zero point. If it were the case, the baryons and antibaryons would continue to annihilate each other as well as annihilate with the nuggets and anti-nuggets in our framework. Eventually it would lead to the Universe with large amount of dark matter in form of nuggets and anti-nuggets (they are far away from each other, therefore they do not annihilate each other) and no visible matter. However, the axion dynamics which is determined by the axion field correlated on the scale of the entire Universe leads to a preferential formation of a specific type of nuggets on the same large scales where the axion field is correlated as we argue below.

First of all we want to argue that the time dependent axion field implies that there is an additional coupling to fermions (3.1). Indeed, by making the time-dependent $U(1)_A$ chiral transformation in the path integral one can always represent the conventional θ term in the following form

$$\Delta\mathcal{L}_4 = \mu_5(t)\bar{\Psi}\gamma_0\gamma_5\Psi \qquad \mu_5 \equiv \dot{\theta}. \tag{3.1}$$

In this formula $\mu_5 \equiv \dot{\theta}$ can be thought as the chiral chemical potential. Many interesting properties emerge in the systems if μ_5 is generated. In fact, it has been an active area of research in recent years, mostly due to very interesting experimental data suggesting that the μ_5 term can be generated in heavy ion collisions, see original paper [52] and recent reviews [53–55] for the details. In the present context the μ_5 term is generated as a result of the axion dynamics. As a matter of fact, the original studies [52] were motivated by the proposal that the separation of the baryon charges which may occur in early Universe, as advocated in this thesis, could be tested in laboratory experiments with heavy ion collisions.

[18] If π meson condensation were occur in nuclear matter it would unambiguously imply that the $\mathcal{CP}$ invariance is broken in such a phase. Some of the phases in CS systems indeed break the $\mathcal{CP}$ invariance as a result of condensation of a pseudo-scalar Nambu-Goldstone bosons.

Now we are prepared to formulate the main claim of this section which can be stated as follows. When interaction (2.10), (3.1) is introduced into the system there will be a *preferential evolution* in the system of the nuggets versus anti-nuggets provided that nuggets and anti-nuggets had been already formed and chemical potential μ had been already generated locally inside the nuggets as described in the previous section 2.4. As we already explained earlier, the generation of μ can be interpreted as a "local violation" of $\mathcal{C}$ invariance in the system.

This *preferential evolution* is correlated with the $\mathcal{CP}$-odd parameter on the scales where the axion field $\theta(x)$ is coherent. In our arguments presented below we make a standard assumption that the initial value of $\theta(x)$ and its time derivative $\dot{\theta}(x)$ are correlated on the entire observable Universe, such that $\mu_5 \equiv \dot{\theta}$ is also correlated on the same large scale. This is the standard assumption in most studies on axion physics when one computes the present density of axions due to the misalignment mechanism and/or the domain wall network decay, see recent papers [9–16, 37].

For our present studies the key element is that the dynamics of the axion field until the QCD phase transition is determined by the coherent state of axions at rest such that [9–16]:

$$\theta(t) \sim \frac{C}{t^{3/4}} \cos \int^t dt' \omega_a(t'), \ \omega_a^2(t) = m_a^2(t) + \frac{3}{16t^2}, \tag{3.2}$$

where C is a constant, and $t = \frac{1}{2H}$ is the cosmic time. This formula suggests that for $m_a(t)t \gg 1$ when the axion potential is sufficiently strongly tilted the chiral chemical potential is essentially determined by the axion mass at time t

$$\mu_5(t) = \dot{\theta}(t) \sim \omega_a(t) \simeq m_a(t). \tag{3.3}$$

The crucial point is that $\theta(t)$ is one and the same in the entire Universe as it is correlated on the Universe size scale. Another important remark is that the axion field $\theta(t)$ continues to oscillate with frequency (3.3) until the QCD phase transition at T_c, though its absolute value $|\theta/\theta_0| \sim 0.01$ might be few orders of magnitude lower at $T_c \simeq 170$ MeV than its original value θ_0 at $T \simeq 1$ GeV when the axion field only started to roll, see e.g. [45]. As we discuss below, the relevant physics is not very sensitive to an absolute value of $|\theta(t)|$ in this regime, and therefore, we do not elaborate further on this rather technical and computational element of the axion dynamics, see footnote 19 below with comments on this matter.

In the context of the nugget's evolution (accretion of the baryon charge) this claim implies that on the entire Universe size scale with one and the

same sign of $\theta(t)$ a specific single type of nuggets will prevail in terms of the number density and sizes. Indeed, one can present the same arguments (see the beginning of this section) with flipping the sign $\mu \to -\mu$ with the only difference is that the interaction (2.10) prevents us from making the variable change $\theta_{(i)} \leftrightarrow -\theta_{(i)}$ for a given $\theta(t)$ because it changes its form under $\theta_{(i)} \leftrightarrow -\theta_{(i)}$. In other words, slow varying (on the QCD scale) $\mathcal{CP}$ violating terms (2.10), (3.1) lead to a preferential evolution of the system for a specific species of the nuggets with a given sign of μ.

Indeed, it has been known for quite some time, see e.g. [56, 57] that in the presence of $\theta \neq 0$ a large number of different $\mathcal{CP}$ violating effects take place. In particular, the Nambu-Goldstone bosons become a mixture of pseudo-scalar and scalar fields, their masses are drastically different from $\theta = 0$ values. Furthermore, the quark chiral $\langle\bar{\psi}\psi\rangle$ and the gluon $\langle G^2\rangle$ condensates become the superposition with their pseudo-scalar counterparts $\langle\bar{\psi}\gamma_5\psi\rangle$ and $\langle G\tilde{G}\rangle$ such that entire hadron spectrum and their interactions modify in the presence of $\theta \neq 0$. All these strong effects, of course, are proportional to θ, and therefore numerically suppressed in case under consideration (3.2) by a factor $|\theta/\theta_0| \sim 10^{-2}$ in the vicinity of the QCD phase transition. Naively, this small numerical factor $|\theta/\theta_0| \sim 10^{-2}$ may lead only to minor effects $\sim 10^{-2}$. However, the crucial point is that while the coupling (2.10) of the axion background field with quarks is indeed relatively small on the QCD scales, it is nevertheless effectively long-ranged and long-lasting in contrast with conventional QCD interactions. As a result, this coherent $\mathcal{CP}$ odd coupling may produce large effects of order of one as we argue below.

Indeed, as we discussed in previous section 2.4 a typical oscillation time $t_{\rm osc}$ when the baryon charge accretes on the wall is of order $t_{\rm osc} \sim m_a^{-1}$ according to eq. (2.44). But this time scale $t_{\rm osc} \sim m_a^{-1}$ is precisely the time scale when $\dot{\theta} = m_a(t)$ varies according to (3.3). Therefore, while the dynamical fermi fields θ_1, θ_2 defined by (2.8) fluctuate with a typical scale of order $\Lambda_{\rm QCD} \gg m_a$, the coherent variation of these fields will occur during a long (on the QCD scales) coherent process when a nugget makes a single cycle. These coherent corrections are expected to be different for nuggets (positive μ) and anti-nuggets (negative μ) as a result of many $\mathcal{C}$ and $\mathcal{CP}$ violating effects such as scattering, transmission, reflection, annihilation, evaporation, mixing of the scalar and pseudo-scalar condensates, etc which are all responsible for the accretion of the baryon charge on a nugget during its long evolution.

Important comment here is that each quark experiences a small difference in interacting with the domain wall surrounding nuggets or anti-nuggets during every single QCD event (mentioned above) with typical QCD time

scale $\Lambda_{\rm QCD}^{-1}$. However, the number of the coherent QCD events $n_{\rm coherent}$ during a long single cycle is very large

$$n_{\rm coherent} \sim \Lambda_{\rm QCD} t_{\rm osc} \sim \frac{\Lambda_{\rm QCD}}{m_a} \sim 10^{10} \gg 1. \tag{3.4}$$

Therefore, a net effect during every single cycle will be order of one, in spite of the fact that each given QCD event is proportional to the axion field $\theta(t)$ and could be quite small.

The argument presented above holds as long as the axion field remains coherent, see also a comment at the very end of this subsection. In other words, a small but non vanishing coherent $\mathcal{CP}$ violating parameter $\theta(t)$ plays the role of catalyst which determines a preferred direction for separation of the baryon charges on the Universe scale. This role of $\mathcal{CP}$ violation in our framework is very different from conventional "baryogenesis" mechanisms when $\mathcal{CP}$ violating parameter explicitly enters the final expression for the baryon charge production.

The corresponding large coherent corrections during a single cycle $t_{\rm osc}$ imply that the fast fluctuating fields θ_1, θ_2 (which effectively describe the dynamics of the fermions living on the wall according to (2.8)) receive large corrections during every single cycle

$$\Delta\theta_1(t) \quad \sim \quad \Delta\theta_2(t) \sim 1. \tag{3.5}$$

These changes of order one of the strongly interacting θ_1, θ_2- fields lead to modification of the accreted baryon charge per single cycle per single degree of freedom

$$\Delta N \sim (\Delta\theta_1 + \Delta\theta_2) \sim 1 \tag{3.6}$$

on the nuggets according to (2.12). One should emphasize that the corrections (3.6) are expected to be different for nuggets and anti-nuggets because the interaction (3.1), (2.10) which is responsible for these corrections (3.6) breaks the symmetry between nuggets and anti-nuggets when $\mu \to -\mu$ as discussed above.

Precise computations of these coherent $\mathcal{CP}$ violating effects are hard to carry out explicitly as it requires a solution of many-body problem of the coherent wall fermions with surrounding environment in the background of axion field (3.2) when a large number of $\mathcal{C}$ and $\mathcal{CP}$ violating effects take place and drastically modify evolution of nuggets versus anti-nuggets. A large number of cycles of every individual nugget (anti-nugget) also introduces a huge uncertainty in computations of ΔN during the time evolution when a

single cycle leads to the effect of order one, with possible opposite sign for a consequent cycle. In other words, it is very hard to predict what would be the final outcome of the system after a large number of cycles when each cycle produces the effect of order 1. We expect that the final result would be again of order one. Such a computation is beyond the scope of the present work. Therefore, in what follows we introduce a phenomenological parameter $c(T)$ of order one to account for these effects. All the observables will be expressed in terms of this single phenomenological parameter $c(T) \sim 1$, see eq. (3.7).

Our final comment in this subsection is as follows. The charge separation effect on largest possible scales is only possible when the axion field (3.2) is coherent on the scales of the Universe. This coherence is known to occur in conventional studies on the dynamics of the axion field in the vicinity of the QCD phase transition [9–14, 16, 45]. At the same time, soon after the QCD phase transition the dominant part of the axion field transfers its energy to the free propagating on-shell axions (which is the subject of axion search experiments [9–14, 16]). These randomly distributed free axions are not in coherent state anymore. Therefore, the coherent accumulation effect which leads to a preferential formation of one species of nuggets, as discussed above, ceases to be operational at the moment of decoherence $t_{\rm dec}$ when the description in terms of the coherent axion field (3.2) breaks down[19]. The baryon asymmetry we observe today in this framework is a result of accumulation of the charge separation effect from the beginning of the nugget's formation until this very last "freeze-out" moment determined by $t_{\rm dec}$.

3.2 Nuggets vs anti-nuggets on the large scale. Generic consequences.

As we already mentioned to make any precise dynamical computations of $\Delta N \sim 1$ due to the coherent axion field (3.2) is a hard problem of strongly coupled QCD at $\theta \neq 0$. In order to effectively account for these coherent effects one can introduce an unknown coefficient $c(T)$ of order one as follows

$$B_{\rm antinuggets} = c(T) \cdot B_{\rm nuggets}, \quad \text{where} \quad |c(T)| \sim 1, \tag{3.7}$$

[19]The decoherence time $t_{\rm dec}$ is not entirely determined by absolute value of amplitude of the axion field (3.2). In fact, the amplitude could be quite small, but the field remains coherent on large scales. The computation of the decoherence time $t_{\rm dec}$ is a hard problem of QFT, similar to a problem in quantum optics when initially coherent light becomes de-coherent superposition of uncorrelated photons.

where $c(T)$ is obviously a negative constant of order one. We emphasize that the main claim of this section represented by eq. (3.7) is not very sensitive to the axion mass $m_a(T)$ nor to the magnitude of $\theta(T)$ at the QCD phase transition when the bubbles start to oscillate and slowly accrete the baryon charge. The only crucial factor in our arguments is that the typical variation of $\theta(t)$ is determined by the axion mass (3.3), which is the same order of magnitude as $t_{\rm osc}^{-1}$, and furthermore, this variation is correlated on the scale where the axion field (3.2) can be represented by the coherent superposition of the axions at rest.

The key relation of this framework (3.7) unambiguously implies that the baryon charge in form of the visible matter can be also expressed in terms of the same coefficient $c(T) \sim 1$ as follows

$$B_{\rm visible} = -B_{\rm antinuggets} - B_{\rm nuggets}. \tag{3.8}$$

Using eq. (3.7) it can be rewritten as

$$\begin{aligned} B_{\rm visible} &\equiv (B_{\rm baryons} + B_{\rm antibaryons}) \\ &= -\left[1 + c(T)\right] B_{\rm nuggets} = -\left[1 + \frac{1}{c(T)}\right] B_{\rm antinuggets}. \end{aligned} \tag{3.9}$$

The same relation can be also represented in terms of the measured observables $\Omega_{\rm visible}$ and $\Omega_{\rm dark}$ at later times when only the baryons (and not antibaryons) contribute to the visible component[20]

$$\Omega_{\rm dark} \simeq \left(\frac{1 + |c(T)|}{|1 + c(T)|}\right) \cdot \Omega_{\rm visible} \quad \text{at} \quad T \leq T_{\rm form}. \tag{3.10}$$

One should emphasize that the relation (3.9) holds as long as the thermal equilibrium is maintained, which we assume to be the case. Another important comment is that each individual contribution $|B_{\rm baryons}| \sim |B_{\rm antibaryons}|$ entering (3.9) is many orders of magnitude greater than the baryon charge hidden in the form of the nuggets and anti-nuggets at earlier times when $T_c > T > T_{\rm form}$. It is just their total baryon charge which is labeled as $B_{\rm visible}$ and representing the net baryon charge of the visible matter is the

[20] In eq. (3.10) we neglect the differences (due to different gaps) between the energy per baryon charge in hadronic and CS phases to simplify notations. The corresponding corrections in energy per baryon charge in hadronic and CS phases, in principle, can be explicitly computed from the first principles. However, we ignore these modifications in the present work. This correction obviously does not change the main claim of this proposal stating that $\Omega_{\rm visible} \approx \Omega_{\rm dark}$.

same order of magnitude (at all times) as the net baryon charge hidden in the form of the nuggets and anti-nuggets according to (3.8).

The baryons continue to annihilate each other (as well as baryon charge hidden in the nuggets) until the temperature reaches $T_{\rm form}$ when all visible antibaryons get annihilated, while visible baryons remain in the system and represent the visible matter we observe today. It corresponds to $c(T_{\rm form}) \simeq -1.5$ as estimated below if one neglects the differences in gaps in CS and hadronic phases, see footnote 20. After this temperature the nuggets essentially assume their final form, and do not loose or gain much of the baryon charge from outside. The rare events of the annihilation between anti-nuggets and visible baryons continue to occur. In fact, the observational excess of radiation in different frequency bands, reviewed in section 1.2, is a result of these rare annihilation events at present time.

The generic consequence of this framework represented by eqs. (3.7), (3.9), (3.10) takes the following form at this time $T_{\rm form}$ for $c(T_{\rm form}) \simeq -1.5$ which corresponds to the case when the nuggets saturate entire dark matter density:

$$\begin{aligned} B_{\rm visible} &\simeq \frac{1}{2} B_{\rm nuggets} \simeq -\frac{1}{3} B_{\rm antinuggets}, \\ \Omega_{\rm dark} &\simeq 5 \cdot \Omega_{\rm visible} \end{aligned} \tag{3.11}$$

which is identically the same relation (1.2) presented in Introduction. The relation (3.11) emerges due to the fact that all components of matter, visible and dark, are proportional to one and the same dimensional parameter $\Lambda_{\rm QCD}$, see footnote 20 with a comment on this approximation. In formula (3.11) $B_{\rm nuggets}$ and $B_{\rm antinuggets}$ contribute to $\Omega_{\rm dark}$, while $B_{\rm visible}$ obviously contributes to $\Omega_{\rm visible}$. The coefficient ~ 5 in relation $\Omega_{\rm dark} \simeq 5 \cdot \Omega_{\rm visible}$ is obviously not universal, but relation (1.1) is universal, and very generic consequence of the entire framework, which was the main motivation for the proposal [4, 5].

For example, if $c(T_{\rm form}) \simeq -2$ then the corresponding relation (3.10) between the dark matter and the visible matter would assume the form $\Omega_{\rm dark} \simeq 3 \cdot \Omega_{\rm visible}$. Such a relation implies that there is a plenty of room for other types of dark matter to saturate the observed ratio $\Omega_{\rm dark}^{\rm observed} \simeq 5 \cdot \Omega_{\rm visible}^{\rm observed}$. This comment will be quite important in our discussions in chapter 4 where we comment on implications of this framework for other axion search experiments.

One should emphasize once again that the generic consequences of the framework represented by (1.1), (3.10) are not sensitive to any specific parameters such as efficiency of the domain wall production or the magnitude

of θ at the QCD phase transition, which could be quite small, see footnote 19 with few comments on that. Nevertheless, precisely the coupling with the coherent $\mathcal{CP}$ odd axion field plays a crucial role in generation of $|c(T)| \neq 1$, i.e. the axion plays the role of catalyst in the baryon charge separation effect on the largest possible scales. Some other observables which are sensitive to the dynamical characteristics (e.g. efficiency of the domain wall production) will be discussed below.

3.3 n_B/n_γ ratio. Model dependent estimates.

The time evolution of the dark matter within this framework is amazingly simple. The relations (3.7), (3.8), (3.9) hold at all times. The baryon charges of the nuggets and anti-nuggets vary until its radius $R(T)$ assumes its equilibrium value as described in sections 2.3, 2.4. It happens approximately at time when the CS phase forms in interior of the nuggets, which can be estimated as $T_{CS} \simeq 0.6\Delta \simeq 60$ MeV, where $\Delta \simeq 100$ MeV is the gap of the CS phase. After this temperature the nuggets essentially assume their final form, with very little variation in size (and baryon charge). The rare events of the annihilation of course continue to occur even for lower tempearures. In fact, the observational consequences reviewed in section 1.2 is a result of these annihilation events at present time.

The variation of the visible matter $B_{\rm visible}$ demonstrates much more drastic changes after the QCD phase transition at T_c because the corresponding number density is proportional to $\exp(-m_N/T)$ such that at the moment of formation $T_{\rm form} \approx 40$ MeV the baryon to entropy ratio assumes its present value (1.5) which we express as follows

$$\eta \equiv \frac{n_B}{n_\gamma} \simeq \frac{B_{\rm visible}/V}{n_\gamma} \sim 10^{-10}, \quad n_B \equiv \frac{B_{\rm visible}}{V}. \tag{3.12}$$

If the nuggets and anti-nuggets were not present at this temperature the conventional baryons and antibaryons would continue to annihilate each other until the density would be 9 orders of magnitude smaller than observed (3.12) when the temperature will be around $T \simeq 22$ MeV. Conventional baryogenesis resolves this "annihilation catastrophe" by producing extra baryons in early times, see e.g. review [20], while in our framework extra baryons and antibaryons are hidden in form of the macroscopically large nuggets.

In our framework the ratio (3.12) can be rewritten in terms of the nugget's density as the baryon charge in form of the visible matter and

in form of the nuggets are related to each other according to (3.9). This relation allows us to infer what efficiency is required for the bubbles to be formed and survive until the present time when the observed ratio is measured (3.12).

One should emphasize that any small factors which normally enter the computations in conventional baryogenesis (such as $\mathcal{C}$ and $\mathcal{CP}$ violating parameters) do not enter in the estimates presented below in our framework as a result of two effects. First, the $\mathcal{C}$ violation enters the computation as a result of generation of the chemical potential μ as described in section 2.2. It is expressed in terms of spontaneous accretion of the baryon charge on the surface of the nuggets as given by eq. (2.12) which effectively generates the chemical potential (2.25), which can be thought as the local violation of the symmetry on the scale of a single nugget. Secondly, the $\mathcal{CP}$ violation enters the computation in form of the coupling with the coherent axion field (3.1). Precisely this coupling as we argued above leads to removing of the degeneracy between nuggets and anti-nuggets formally expressed as $c(T) \sim 1$ in eq. (3.7). Therefore, the only small parameter we anticipate in our estimates below is due to some suppression of the closed bubbles which must be formed with sufficiently large sizes during the QCD phase transition.

We cannot compute the probability for the bubble formation as it obviously requires the numerical simulations, which is beyond the scope of the present work. Instead, we go backward and ask the question: What should be the efficiency of the bubble formation at the QCD phase transition in order to accommodate the observed ratio (3.12)?

With these comments in mind we proceed with our estimates as follows. First, from (3.9), (3.11) we infer that the baryon charge hidden in the nuggets and anti-nuggets is the same order of magnitude as the baryon charge of the visible baryons at $T_{\rm form}$ at the end of the formation, i.e.

$$\frac{B_{\rm nuggets}/V}{n_\gamma} \gtrsim 10^{-10}, \tag{3.13}$$

where we use sign $\gtrsim$ instead of $\approx$ used in eq (3.12) to emphasize that there is long time for equilibration between the moment $T_{\rm CS} \simeq 0.6\Delta \simeq 60$ MeV when CS phase forms in interior of the nuggets and $T_{\rm form} \simeq 40$ MeV when all antibaryons of the visible matter get annihilated, corresponding to the present observed value (3.12). During this period the equilibrium between the visible matter and the baryons from nuggets is maintained, and some portion of the nugget's baryon charge might be annihilated by the visible matter. It explains our sign $\gtrsim$ used in eq. (3.13).

The relation (3.13) implies that the number density of nuggets and anti-nuggets can be estimated as

$$\frac{\langle B\rangle n_{\rm nuggets}}{n_\gamma} \gtrsim 10^{-10}, \quad \langle B\rangle n_{\rm nuggets} \equiv \frac{B_{\rm nuggets}}{V}, \tag{3.14}$$

where $\langle B\rangle$ is the average baryon charge of a single nugget at $T_{\rm form}$.

Now we want to estimate the same ratio (3.14) using the Kibble-Zurek (KZ) mechanism[41–43] reviewed in section 2.1. The basic idea of the KZ mechanism is that the total area of the crumpled, twisted and folded domain wall is proportional to the volume of the system, and can be estimated as follows:

$$S_{(\text{total DW})} = \frac{V}{\xi(T)}, \tag{3.15}$$

where $\xi(T)$ is the correlation length which is defined as an average distance between crumpled domain walls at temperature T. Largest part of the wall belongs to the percolated large cluster. It is known that some closed walls (bubbles) with typical size $\xi(T)$ will be also formed. These bubbles with sufficiently large size $R \sim \xi(T)$ will eventually become nuggets. We introduce parameter γ to account for the suppression related to the closed bubble formation. In other words, we define

$$S_{\rm nuggets} = \gamma S_{(\text{total DW})} = \frac{\gamma V}{\xi(T)}, \quad \gamma \ll 1. \tag{3.16}$$

At the same time total area of the nuggets $S_{\rm nuggets}$ can be estimated as

$$S_{\rm nuggets} = 4\pi R_0^2(T)\left[V \cdot n_{\rm nuggets}\right], \tag{3.17}$$

where R_0 is the size of a nuggets at initial time, while $[V \cdot n_{\rm nuggets}]$ represents the total number of nuggets in volume V. Comparison of (3.16) with (3.17) gives the following estimate for the nugget's density when bubbles just formed,

$$n_{\rm nuggets} \simeq \frac{\gamma}{4\pi R_0^2 \xi}. \tag{3.18}$$

The last step in our estimates is the computation of the average baryon charge of a nugget at $T_{\rm CS}$ when CS sets in inside the nugget. The corresponding estimates have been worked out long ago [4] and reproduced in section 2.3 in the course of the time evolution by taking $t \to \infty$, see

(2.26). The baryon number density inside the nuggets depends on a model being used [4], but typically it is few times the nuclear saturation density $n_0 \simeq (108\ \mathrm{MeV})^3$ which is consistent with conventional computations for the baryon density in CS phases. Therefore, we arrive to

$$\langle B \rangle \simeq (2-6) n_0 \cdot \frac{4\pi R_{\rm form}^3}{3}, \tag{3.19}$$

where $R_{\rm form}$ is the final size of the nuggets. By substituting (3.19) and (3.18) to (3.14) we arrive to the following constraint on efficiency of the bubble formation represented by parameter γ

$$(2-6) \cdot \frac{\gamma}{3} \left(\frac{R_{\rm form}}{\xi(T)}\right) \left(\frac{R_{\rm form}}{R_0}\right)^2 \left(\frac{n_0}{n_\gamma}\right) \gtrsim 10^{-10}, \tag{3.20}$$

where expression for $n_\gamma(T)$ should be taken at the formation time

$$n_\gamma = \frac{2\xi(3)}{\pi^2} T_{\rm form}^3, \quad \xi(3) \simeq 1.2, \tag{3.21}$$

while the correlation length $\xi(T)$ should be evaluated at much earlier times, close to T_c when domain wall network only started to form. Typically bubbles form with $R_0 \sim \xi$. However, the bubbles shrink approximately 3-5 times according to (2.43) before they reach equilibrium during the time evolution as discussed in section 2.4. Therefore, to be on a safe side, we make very conservative assumption that

$$\frac{R_{\rm form}}{R_0} \sim 0.1, \quad R_0 \simeq \xi. \tag{3.22}$$

To proceed with numerical estimates, it is convenient to factor γ on two pieces,

$$\gamma \equiv \gamma_{\rm formation} \cdot \gamma_{\rm evolution}, \qquad \gamma_{\rm formation} \sim 0.1, \tag{3.23}$$

where the first part, $\gamma_{\rm formation} \sim 0.1$ has been estimated using numerical simulations, see textbook [43] for review. The second suppression factor $\gamma_{\rm evolution}$ is unknown, and includes a large number of different effects. In particular, many small closed bubbles with $R_0 \leq \xi$ are very likely to be formed but may not survive the evolution as we discussed in section 2.4. Furthermore, there are many effects such as evaporation, annihilation inside the nuggets which may also lead to collapse of relatively small nuggets. Furthermore, the formation probability of large closed bubbles with $R_0 \gg \xi$

(which are most likely to survive) is highly suppressed $\sim \exp(-R_0^2/\xi^2)$. All these effects are included in the unknown parameter $\gamma_{\rm evolution}$. Our constraint (from observations on n_B/n_γ within our mechanism) can be inferred from (3.20)

$$\gamma_{\rm evolution}(T_{\rm form}) \gtrsim 10^{-7}. \tag{3.24}$$

One suppression factor which obviously contributes to suppression (3.24) is related to necessity to produce a sufficiently large initial bubble for successful nugget formation as given by eq. (2.43). We do not know a numerical value for the correlation length ξ in our system at the initial moment of formation[21]. However, even in the worst case scenario when $R_0 \sim 3\xi$ instead of $R_0 \sim \xi$, which is normally assumed in KZ simulations, the corresponding suppression factor

$$\exp\left(-\frac{R_0^2}{\xi^2}\right) \sim 10^{-4} \tag{3.25}$$

is still perfectly consistent with the observational constraint (3.24).

We emphasize that there is no fine tuning in this estimate and overshooting the estimate (3.24) is perfectly consistent with constraint (3.24). This is because the equilibration of the baryon charge from the nuggets with the visible baryons always lead to the result (1.1), (3.9) when all contributions are the same order of magnitude. The precise ratio (3.12), as we already mentioned, is determined by the moment in evolution of the Universe when all visible baryons get completely annihilated which is the formation temperature $T_{\rm form} \sim \Lambda_{\rm QCD}$, which is again, perfectly consistent with the main paradigm of the entire framework that all dimensional parameters are order of $\Lambda_{\rm QCD}$.

How one can understand the result (3.24) which essentially states that even very tiny probability of the formation of the closed bubbles is still sufficient to saturate the observed ratio (3.12)? The answer lies in the observation that the baryon density $n_B \simeq n_{\bar{B}}$ was 10 orders of magnitude larger at the moment of the bubble formation. Therefore, even a tiny probability at the moment of formation of a closed bubble with sufficiently large size will lead to effects of order one at the moment when the baryon number density drops 10 order in magnitude. Another reason why very tiny

[21] One should emphasize that the correlation length ξ should not be identified with $R_{\rm form}$ when the nugget's formation is almost completed. Rather the correlation length ξ, defined by (3.15), characterizes the system at the very beginning of the formation when the domain wall network starts to emerge. It is normally assumed that $\xi \simeq R_0$. Most likely R_0 should be slightly greater than ξ for successful formation.

probability of the formation of the closed bubbles nevertheless is sufficient to saturate the observed ratio (3.12) is that typical "small factors" which normally accompany the conventional baryogenesis mechanisms such as $\mathcal{CP}$ and $\mathcal{C}$ odd couplings do not appear in estimate (3.24) due to the reasons already explained after eq (3.12).

• We conclude this section with the following comment: The basic consequences of this framework represented by eqs. (1.1), (3.9), (3.10) are very generic. These features are not very sensitive to efficiency of the closed domain wall formation (as long as it is greater than (3.24)) nor to the absolute value of θ as long as coherence is maintained, see footnote 19. These generic features hold for arbitrary value of the axion mass $10^{-6}\text{eV} \leq m_a \leq 10^{-3}\text{eV}$, in contrast with conventional treatment of the axion as the dark matter candidate, when $\Omega_{\rm DM}$ can be saturated by the axions only when the axion mass assumes a very specific and definite value $m_a \simeq 10^{-6}$ eV, see next section with details.

The derivation of the observed ratio (3.12) from the first principles (which is entirely determined by $T_{\rm form}$) is a hard computational problem of strongly coupled QCD when all elements such as cooling rate, annihilation rate, charge separation rate, damping rate, evaporation rate and many other effects are equally contribute to $T_{\rm form}$. However, it is important that the "observational" value $T_{\rm form}$ lies precisely in the region where it should be: $T_{\rm form} < T_{\rm CS}$, i.e. slightly below the temperature where CS sets in. Therefore, any fine-tuning procedures have never been required in this framework (in contrast with conventional baryogenesis computations) to accommodate the observed ratios presented by eqs. (1.1), (3.12).

Chapter 4

Implications for the Axion Search Experiments

The goal of this section is to comment on relation of our framework and the direct axion search experiments [9–16]. We start with the following comment we made in section 1.2: this model which has a single fundamental parameters (a mean baryon number of a nugget $\langle B\rangle \sim 10^{25}$ entering all the computations) is consistent with all known astrophysical, cosmological, satellite and ground based constraints as reviewed in section 1.2. For discussions of this section it is convenient to express this single normalization parameter $\langle B\rangle \sim 10^{25}$ in terms of the axion mass $m_a \sim 10^{-4}$ eV as these two parameters are directly related according to the scaling relations (1.3). The corresponding relation between these two parameters occur because the axion mass m_a determines the wall tension $\sigma \sim m_a^{-1}$ which itself enters the expression for the equilibrium value of the size of the nuggets, $R_{\rm form}$ at the end of the formation. One should emphasize that it is quite nontrivial that the cosmological constraints on the nuggets as shown on Fig. 1.2 and formulated in terms of $\langle B\rangle$ are compatible with known upper limit on the axion mass $m_a < 10^{-3}$eV within our framework. One could regard this compatibility as a nontrivial consistency check for this proposal.

The lower limit on the axion mass, as it is well known, is determined by the requirement that the axion contribution to the dark matter density does not exceed the observed value $\Omega_{\rm dark} \approx 0.23$. There is a number of uncertainties in the corresponding estimates. We shall not comment on these subtleties by referring to the review papers[9–16]. The corresponding uncertainties are mostly due to the remaining discrepancies between different groups on the computations of the axion production rates due to the different mechanisms such as misalignment mechanism versus domain wall/string decays. In what follows to be more concrete in our estimates we shall use the following expression for the dark matter density in terms of the axion

mass resulted from the misalignment mechanism [16]:

$$\Omega_{(\text{DM axion})} \simeq \left(\frac{6\cdot 10^{-6}\text{eV}}{m_a}\right)^{\frac{7}{6}} \tag{4.1}$$

This formula essentially states that the axion of mass $m_a \simeq 2\cdot 10^{-5}$ eV saturates the dark matter density observed today, while the axion mass in the range of $m_a \geq 10^{-4}$ eV contributes very little to the dark matter density. This claim, of course, is entirely based on estimate (4.1) which accounts only for the axions directly produced by the misalignment mechanism suggested originally in [47].

There is another mechanism of the axion production when the Peccei-Quinn symmetry is broken after inflation. In this case the string-domain wall network produces a large number of axions such that the axion mass $m_a \simeq 10^{-4}$ eV may saturate the dark matter density, see relatively recent estimates [45, 46] with some comments and references on previous papers. The corresponding formula from refs.[45, 46] is also highly sensitive to the axion mass with m_a- dependence being very similar to eq. (4.1).

The main lesson to be learnt from the present work is that in addition to these well established mechanisms previously discussed in the literature there is an additional contribution to the dark matter density also related to the axion field. However, the mechanism which is advocated in the present work contributes to the dark matter density through formation of the nuggets, rather than through the direct axion production. The corresponding mechanism as argued in section 3.2 always satisfies the relation $\Omega_{\text{dark}} \approx \Omega_{\text{visible}}$, and, in principle is capable to saturate the dark matter density $\Omega_{\text{dark}} \approx 5\Omega_{\text{visible}}$ by itself for arbitrary magnitude of the axion mass m_a as the corresponding contribution is not sensitive to the axion mass in contrast with conventional mechanisms mentioned above. A precise coefficient in ratio $\Omega_{\text{dark}} \approx \Omega_{\text{visible}}$ is determined by a parameter of order one, $|c(T)| \sim 1$, which unfortunately is very hard to compute from the first principles, as discussed in section 3.2.

Our choice for $m_a \simeq 10^{-4}$ eV which corresponds to $\langle B\rangle \sim 10^{25}$ is entirely motivated by our previous analysis of astrophysical, cosmological, satellite and ground based constraints as reviewed in Section 1.2. As we mentioned in Section 1.2 there is a number of frequency bands where some excess of emission was observed, and this model may explain some portion, or even entire excess of the observed radiation in these frequency bands. Our normalization $\langle B\rangle \sim 10^{25}$ was fixed by eq.(1.6) with assumption that the observed dark matter is saturated by the nuggets. The relaxing of this

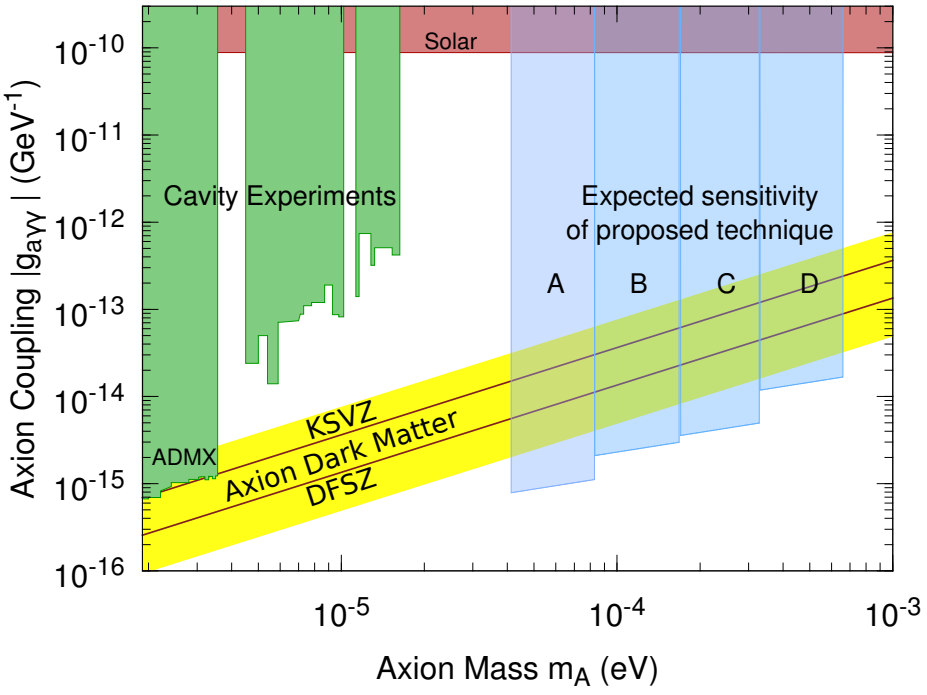

Figure 4.1: Cavity / ADMX experimental constraints on the axion mass shown in green. The expected sensitivity for the Orpheus axion search experiment [15] is shown by blue regions "A", "B", "C" and "D". In particular, experiment "B", covers the most interesting region of the parametrical space with $m_a \simeq 10^{-4}$ eV corresponding to the nuggets with mean baryon charge $\langle B \rangle \simeq 10^{25}$ which itself satisfies all known astrophysical, cosmological, satellite and ground based constraints, see Fig.1.2. The plot is taken from [15].

assumption obviously modifies the coefficient $c(T)$ as well as $\langle B \rangle$.

Interestingly enough, this range of the axion mass $m_a \simeq 10^{-4}$ eV is perfectly consistent with recent claim [58],[59] that the previously observed small signal in resonant S/N/S Josephson junction [60] is a result of the dark matter axions with the mass $m_a \simeq 1.1 \cdot 10^{-4}$ eV. Furthermore, it has been also claimed that similar anomalies have been observed in other experiments [61–63] which all point towards an axion mass $m_a \simeq 1.1 \cdot 10^{-4}$ eV if interpreted within framework [58],[59]. The only comment we would like to make here is that if the interpretation [58],[59] of the observed anomalies [60–63] is indeed due to the dark matter axions, then the corresponding axion mass is perfectly consistent with our estimates (based on cosmological observations) of the average baryon charge of the nuggets $\langle B \rangle \simeq 10^{25}$ as reviewed in section 1.2.

We conclude this section on an optimistic note with a remark that the most interesting region of the parametric space corresponding to the nuggets with mean baryon charge $\langle B \rangle \simeq 10^{25}$ might be tested by the Orpheus axion search experiment [15] as shown on Fig. 4.1.

Chapter 5

Conclusion

First, we want to list the main results of the present studies, while the comments on possible future developments will be presented at the end of this chapter.

1. First key element of this proposal is the observation (2.12) that the closed axion domain walls are copiously produced and generically will acquire the baryon or antibaryon charge. This phenomenon of "separation of the baryon charge" can be interpreted as a local version of spontaneous symmetry breaking. This symmetry breaking occurs not in the entire volume of the system, but on the correlation length $\xi(T) \sim m_a^{-1}$ which is determined by the folded and crumpled axion domain wall during the formation stage. Precisely this local charge separation eventually leads to the formation of the nuggets and anti-nuggets serving in this framework as the dark matter component $\Omega_{\rm dark}$.

2. Number density of nuggets and anti-nuggets will not be identically the same as a result of the coherent (on the scale of the Universe) axion $\mathcal{CP}$ -odd field. We parameterize the corresponding effects of order one by phenomenological constant $c(T) \sim 1$. It is important to emphasize that this parameter of order one is not a fundamental constant of the theory, but, calculable from the first principles. In practice, however, such a computation could be quite a challenging problem when even the QCD phase diagram is not known. The fundamental consequence of this framework, $\Omega_{\rm dark} \approx \Omega_{\rm visible}$, which is given by (1.1) is *universal*, and not sensitive to any parameters as both components are proportional to $\Lambda_{\rm QCD}$. The observed ratio (1.2), (3.11) corresponds to a specific value of $c(T_{\rm form}) \simeq -1.5$ as discussed in section 3.2.

3. Another consequence of the proposal is a natural explanation of the ratio (1.5) in terms of the formation temperature $T_{\rm form} \simeq 40$ MeV, rather than in terms of specific coupling constants which normally enter conventional "baryogenesis" computations. This observed ratio is expressed in our framework in terms of a single parameter $T_{\rm form}$ when the nuggets complete their formation. This parameter is not fundamental constant of the theory, and as such is calculable from the first principles. In practice, however, the

computation of $T_{\rm form}$ is quite a challenging problem as explained in section 3.3. Numerically, the observed ratio (1.5) corresponds to $T_{\rm form} \simeq 40$ MeV which is indeed slightly below the critical temperature $T_{CS} \simeq 60$ MeV where the colour superconductivity sets in.

The relation $T_{\rm form} \lesssim T_{CS} \sim \Lambda_{\rm QCD}$ is *universal* in this framework as both parameters are proportional to $\Lambda_{\rm QCD}$. As such, the universality of this framework is similar to the universality $\Omega_{\rm dark} \approx \Omega_{\rm visible}$ mentioned in previous item. At the same time, the ratio (1.5) is not universal itself as it is exponentially sensitive to precise value of $T_{\rm form}$ due to conventional suppression factor $\sim \exp(-m_p/T)$.

4. The only new fundamental parameter of this framework is the axion mass m_a. Most of our computations (related to the cosmological observations, see section 1.2 and Fig. 1.2), however, are expressed in terms of the mean baryon number of nuggets $\langle B\rangle$ rather than in terms of the axion mass. However, these two parameters are unambiguously related according to the scaling relations (1.3). Our claim is that all *universal* properties of this framework listed above still hold for any m_a. In other words, there is no any fine tuning in the entire construction with respect to m_a. The constraints (and possible cosmological observations) from section 1.2 strongly suggest $\langle B\rangle \simeq 10^{25}$ which can be translated into preferred value for the axion mass $m_a \simeq 10^{-4}$ eV.

5. This region of the axion mass $m_a \simeq 10^{-4}$ eV corresponding to average size of the nuggets $\langle B\rangle \simeq 10^{25}$ can be tested in the Orpheus axion search experiment [15] as shown on Fig. 4.1.

We conclude with few thoughts on future directions within our framework. It is quite obvious that future progress cannot be made without a much deeper understanding of the QCD phase diagram at $\theta \neq 0$. In other words, we need to understand the structure of possible phases along the third dimension parametrized by θ on Fig 1.1.

Presently, very few results are available regarding the phase structure at $\theta \neq 0$. First of all, the phase structure is understood in simplified version of QCD with two colours, $N_c = 2$ at $T = 0, \mu \neq 0$, see [64]. In fact, the studies [64] were mostly motivated by the subject of the present work and related to the problem of formation of the quark nuggets during the QCD phase transition in early Universe with non vanishing θ. With few additional assumptions the phase diagram can be also conjectured for the system with large number of colours $N_c = \infty$, at non vanishing T, μ, θ, see [65, 66].

Due to the known "sign problem", see footnote 2, the conventional lattice simulations cannot be used at $\theta \neq 0$. The corresponding analysis of the phase diagram for non vanishing θ started just recently by using some newly

invented technical tricks [67–70].

Another possible development from the "wish list" is a deeper understanding of the closed bubble formation. Presently, very few results are available on this topic. The most relevant for our studies is the observation made in [11] that a small number of closed bubbles are indeed observed in numerical simulations. However, their detailed properties (their fate, size distribution, etc) have not been studied yet. A number of related questions such as an estimation of correlation length $\xi(T)$, the generation of the structure inside the domain walls, the baryon charge accretion on the bubble, etc, hopefully can be also studied in such numerical simulations.

One more possible direction for future studies from the "wish list" is a development some QCD-based models where a number of hard questions such as: evolution of the nuggets, cooling rates, evaporation rates, annihilation rates, viscosity of the environment, transmission/reflection coefficients, etc in unfriendly environment with non-vanishing T, μ, θ can be addressed, and hopefully answered. All these and many other effects are, in general, equally contribute to our parameters $T_{\rm form}$ and $c(T)$ at the $\Lambda_{\rm QCD}$ scale in strongly coupled QCD. Precisely these numerical factors eventually determine the coefficients in the observed relations: $\Omega_{\rm dark} \approx \Omega_{\rm visible}$ given by eq. (3.10) and n_B/n_γ expressed by eq. (3.12).

Last but not least: the discovery of the axion in the Orpheus experiment [15] would conclude a long and fascinating journey of searches for this unique and amazing particle conjectured almost 40 years ago. Such a discovery would be a strong motivation for related searches of "something else" as the axion mass $m_a \simeq 10^{-4}$ is unlikely to saturate the dark matter density observed today. We advocate the idea that this "something else" is the "quark nuggets" (where the axion plays the key role in entire construction) which could provide the principle contribution to dark matter of the Universe as the relation $\Omega_{\rm dark} \approx \Omega_{\rm visible}$ in this framework is not sensitive to the axion mass.

Bibliography

[1] D. S. Akerib, H. M. Araújo, X. Bai, A. J. Bailey, J. Balajthy, P. Beltrame, E. P. Bernard, A. Bernstein, T. P. Biesiadzinski, E. M. Boulton, A. Bradley, R. Bramante, S. B. Cahn, M. C. Carmona-Benitez, C. Chan, J. J. Chapman, A. A. Chiller, C. Chiller, A. Currie, J. E. Cutter, T. J. R. Davison, L. de Viveiros, A. Dobi, J. E. Y. Dobson, E. Druszkiewicz, B. N. Edwards, C. H. Faham, S. Fiorucci, R. J. Gaitskell, V. M. Gehman, C. Ghag, K. R. Gibson, M. G. D. Gilchriese, C. R. Hall, M. Hanhardt, S. J. Haselschwardt, S. A. Hertel, D. P. Hogan, M. Horn, D. Q. Huang, C. M. Ignarra, M. Ihm, R. G. Jacobsen, W. Ji, K. Kazkaz, D. Khaitan, R. Knoche, N. A. Larsen, C. Lee, B. G. Lenardo, K. T. Lesko, A. Lindote, M. I. Lopes, D. C. Malling, A. Manalaysay, R. L. Mannino, M. F. Marzioni, D. N. McKinsey, D.-M. Mei, J. Mock, M. Moongweluwan, J. A. Morad, A. St. J. Murphy, C. Nehrkorn, H. N. Nelson, F. Neves, K. O'Sullivan, K. C. Oliver-Mallory, R. A. Ott, K. J. Palladino, M. Pangilinan, E. K. Pease, P. Phelps, L. Reichhart, C. Rhyne, S. Shaw, T. A. Shutt, C. Silva, V. N. Solovov, P. Sorensen, S. Stephenson, T. J. Sumner, M. Szydagis, D. J. Taylor, W. Taylor, B. P. Tennyson, P. A. Terman, D. R. Tiedt, W. H. To, M. Tripathi, L. Tvrznikova, S. Uvarov, J. R. Verbus, R. C. Webb, J. T. White, T. J. Whitis, M. S. Witherell, F. L. H. Wolfs, K. Yazdani, S. K. Young, and C. Zhang. Improved limits on scattering of weakly interacting massive particles from reanalysis of 2013 lux data. *Phys. Rev. Lett.*, 116:161301, Apr 2016.

[2] E. Witten, Phys. Rev. D **30**, 279 (1984).

[3] E. Farhi and R. Jaffe, Phys. Rev.**D 30** (1984) 1601; Phys. Rev.**D 30** (1984) 2379.
C. Alcock and E. Farhi, Phys. Rev. **D32** (1985) 1273;
J. Madsen, H. Heiselberg and K. Riisager, Phys. Rev. **D34** (1986) 2947;
C. Alcock and A. Olinto, Phys. Rev. **D39** (1989) 1233.

[4] A. R. Zhitnitsky, JCAP **0310**, 010 (2003) [hep-ph/0202161].

[5] D. H. Oaknin and A. Zhitnitsky, Phys. Rev. D **71**, 023519 (2005) [hep-ph/0309086].

[6] R. D. Peccei and H. R. Quinn, Phys. Rev. D **16**, 1791 (1977);
S. Weinberg, Phys. Rev. Lett. **40**, 223 (1978);
F. Wilczek, Phys. Rev. Lett. **40**, 279 (1978).

[7] J.E. Kim, Phys. Rev. Lett. **43** (1979) 103;
M.A. Shifman, A.I. Vainshtein, and V.I. Zakharov, Nucl. Phys. **B166** (1980) 493(KSVZ-axion).

[8] M. Dine, W. Fischler, and M. Srednicki, Phys. Lett. **B104** (1981) 199;
A.R. Zhitnitsky, Yad.Fiz. **31** (1980) 497; Sov. J. Nucl. Phys. **31** (1980) 260 (DFSZ-axion).

[9] K. van Bibber and L. J. Rosenberg, Phys. Today **59N8**, 30 (2006);

[10] S. J. Asztalos, L. J. Rosenberg, K. van Bibber, P. Sikivie, K. Zioutas, Ann. Rev. Nucl. Part. Sci. **56**, 293-326 (2006).

[11] Pierre Sikivie, arXiv:0610440v2 [astro-ph].

[12] G. G. Raffelt, Lect. Notes Phys. **741**, 51 (2008) [hep-ph/0611350].

[13] P. Sikivie, Int. J. Mod. Phys. A **25**, 554 (2010) [arXiv:0909.0949 [hep-ph]].

[14] L. J. Rosenberg, Proc. Nat. Acad. Sci. (2015).

[15] G. Rybka, A. Wagner, A. Brill, K. Ramos, R. Percival and K. Patel, Phys. Rev. D **91**, no. 1, 011701 (2015) [arXiv:1403.3121 [physics.ins-det]].

[16] P. W. Graham, I. G. Irastorza, S. K. Lamoreaux, A. Lindner and K. A. van Bibber, Ann. Rev. Nucl. Part. Sci. **65**, 485 (2015) [arXiv:1602.00039 [hep-ex]].

[17] M. G. Alford, A. Schmitt, K. Rajagopal and T. Schäfer, Rev. Mod. Phys. **80**, 1455 (2008) [arXiv:0709.4635 [hep-ph]]

[18] K. Rajagopal and F. Wilczek, In *Shifman, M. (ed.): At the frontier of particle physics, vol. 3* 2061-2151 [hep-ph/0011333].

[19] A. D. Sakharov, JETP Lett. **5**, 24 (1967).

[20] A. D. Dolgov, "Baryogenesis, 30 years after," hep-ph/9707419.

[21] A. Zhitnitsky, Phys. Rev. D **74**, 043515 (2006) [astro-ph/0603064].

[22] D. H. Oaknin and A. R. Zhitnitsky, Phys. Rev. Lett. **94**, 101301 (2005), arXiv:hep-ph/0406146.

[23] A. Zhitnitsky, Phys. Rev. D **76**, 103518 (2007), arXiv:astro-ph/0607361.

[24] K. Lawson and A. R. Zhitnitsky, JCAP **0801**, 022 (2008), arXiv:0704.3064 [astro-ph].

[25] M. M. Forbes, K. Lawson and A. R. Zhitnitsky, Phys. Rev. D **82**, 083510 (2010) [arXiv:0910.4541 [astro-ph.GA]].

[26] M. M. Forbes and A. R. Zhitnitsky, JCAP **0801**, 023 (2008) [astro-ph/0611506].

[27] M. M. Forbes and A. R. Zhitnitsky, Phys. Rev. D **78**, 083505 (2008) [arXiv:0802.3830 [astro-ph]].

[28] K. Lawson and A. R. Zhitnitsky, Phys. Lett. B **724**, 17 (2013) [arXiv:1210.2400 [astro-ph.CO]].

[29] K. Lawson, Phys. Rev. D **83**, 103520 (2011) [arXiv:1011.3288 [astro-ph.HE]].

[30] K. Lawson, Phys. Rev. D **88**, no. 4, 043519 (2013) [arXiv:1208.0042 [astro-ph.HE]].

[31] K. Lawson and A. R. Zhitnitsky, eProceedings for Cosmic Frontier Workshop: Snowmass 2013 Menlo Park, USA, March 6-8, 2013, [arXiv:1305.6318 [astro-ph.CO]].

[32] E. S. Abers, A. K. Bhatia, D. A. Dicus, W. W. Repko, D. C. Rosenbaum and V. L. Teplitz, Phys. Rev. D **79**, 023513 (2009) [arXiv:0712.4300 [astro-ph]].

[33] P. W. Gorham, Phys. Rev. D **86**, 123005 (2012) [arXiv:1208.3697 [astro-ph.CO]].

[34] P. W. Gorham and B. J. Rotter, arXiv:1507.03545 [astro-ph.CO].

[35] K. Lawson and A. R. Zhitnitsky, Phys. Lett. B **757**, 376 (2016) [arXiv:1510.02092 [astro-ph.GA]].

[36] K. Lawson and A. R. Zhitnitsky, arXiv:1510.07646 [astro-ph.HE].

[37] P. Sikivie, Phys. Rev. Lett. **48** (1982) 1156;
A. Vilenkin and A.E. Everett, Phys. Rev. Lett. **48** (1982) 1867.

[38] M. M. Forbes and A. R. Zhitnitsky, JHEP **0110**, 013 (2001) [arXiv:hep-ph/0008315].

[39] G. Gabadadze and M.A. Shifman, Phys. Rev.**D 62**(2000)114003 [arXiv:hep-ph/0007345].

[40] D. T. Son, M. A. Stephanov and A. R. Zhitnitsky, Phys. Rev. Lett. **86**, 3955 (2001) [hep-ph/0012041].

[41] T.W.B. Kibble, J. Phys. A9, 1387 (1976);
W. Zurek, Nature **317**, 505 (1985)

[42] W. Zurek, Phys. Rep. **276**, 177 (1996)

[43] A. Vilenkin, E.P.S. Shellard, "Cosmic strings and other topological defects", Cambridge University Press, 1994

[44] S. Chang, C. Hagmann and P. Sikivie, Phys. Rev. D **59**, 023505 (1999) [hep-ph/9807374].

[45] O. Wantz and E. P. S. Shellard, Phys. Rev. D **82**, 123508 (2010) [arXiv:0910.1066 [astro-ph.CO]].
O. Wantz and E. P. S. Shellard, Nucl. Phys. B **829**, 110 (2010) [arXiv:0908.0324 [hep-ph]].

[46] M. Kawasaki, K. Saikawa and T. Sekiguchi, Phys. Rev. D **91**, no. 6, 065014 (2015) [arXiv:1412.0789 [hep-ph]].

[47] J. Preskill, M. B. Wise, and F. Wilczek, Phys.Lett. **B120**, 127 (1983);
L. Abbott and P. Sikivie, Phys.Lett. B **120**, 133 (1983);
M. Dine and W. Fischler, Phys.Lett. B **120**, 137 (1983).

[48] M. M. Forbes and A. R. Zhitnitsky, Phys. Rev. Lett. **85**, 5268 (2000) [hep-ph/0004051], hep-ph/0102158.

[49] S. Mandelstam, Phys. Rev. D**11**, 3026 (1975).

[50] S. Coleman, Phys. Rev. D**11**, 2088 (1975).

[51] R. Jackiw and C. Rebbi, Phys. Rev. D **13**, 3398 (1976). doi:10.1103/PhysRevD.13.3398

[52] D. Kharzeev and A. Zhitnitsky, Nucl. Phys. A **797**, 67 (2007) [arXiv:0706.1026 [hep-ph]].

[53] D. E. Kharzeev, Annals Phys. **325**, 205 (2010) [arXiv:0911.3715 [hep-ph]].

[54] D. E. Kharzeev, Prog. Part. Nucl. Phys. **75**, 133 (2014) [arXiv:1312.3348 [hep-ph]].

[55] D. E. Kharzeev, J. Liao, S. A. Voloshin and G. Wang, Prog. Part. Nucl. Phys. **88**, 1 (2016) [arXiv:1511.04050 [hep-ph]].

[56] I. E. Halperin and A. Zhitnitsky, Phys. Rev. Lett. **81**, 4071 (1998) [hep-ph/9803301].

[57] T. Fugleberg, I. E. Halperin and A. Zhitnitsky, Phys. Rev. D **59**, 074023 (1999) [hep-ph/9808469].

[58] C. Beck, Phys. Rev. Lett. **111**, 231801 (2013), [arxiv:1309.3790[hep-ph]];

[59] C. Beck, [arxiv:1403.5676 [hep-ph]]

[60] C. Hoffmann et al, Phys. Rev. B **70**, 180503 (R) (2004)

[61] T.E. Golikova et al, Phys. Rev. B **86**, 064416 (2012)

[62] L. He et al, [arxiv:1107.0061]

[63] M.H. Bae et al, Phys. Rev. B **77**, 144501 (2008)

[64] M. A. Metlitski and A. R. Zhitnitsky, Nucl. Phys. B **731**, 309 (2005) [hep-ph/0508004].

[65] A. Parnachev and A. R. Zhitnitsky, Phys. Rev. D **78**, 125002 (2008) [arXiv:0806.1736 [hep-ph]].

[66] A. R. Zhitnitsky, Nucl. Phys. A **813**, 279 (2008) [arXiv:0808.1447 [hep-ph]].

[67] M. D'Elia and F. Negro, Phys. Rev. D **88**, no. 3, 034503 (2013) [arXiv:1306.2919 [hep-lat]].

[68] C. Bonati, M. D'Elia, H. Panagopoulos and E. Vicari, Phys. Rev. Lett. **110**, no. 25, 252003 (2013) [arXiv:1301.7640 [hep-lat]].

[69] C. Bonati, JHEP **1503**, 006 (2015) [arXiv:1501.01172 [hep-lat]].

[70] C. Bonati, M. D'Elia and A. Scapellato, Phys. Rev. D **93**, no. 2, 025028 (2016) [arXiv:1512.01544 [hep-lat]].

[71] P. B. Arnold, G. D. Moore and L. G. Yaffe, JHEP **0011**, 001 (2000) [hep-ph/0010177].

[72] Jiunn-Wei Chen and Eiji Nakano. Phys. Lett. B **647**, 371 (2007).

Appendix A

Estimation of Fluxes

The main goal of this Appendix is to argue that the approximation in eq. (2.24) which was adopted in the text by neglecting the extra term "fluxes" is justified, at least on qualitative level. In other words, while these "flux" terms are obviously present in the system, they, nevertheless, do not drastically change a key technical element (an implicit relation between $R(t)$ and $\mu(t)$) which this equation provides. Precisely this implicit relation between $R(t)$ and $\mu(t)$ eventually allows us to express the μ-dependent pressure $\Delta P[\mu]$ in terms of R dependent function $\Delta P[f(R)]$ such that the basic equation (2.37) describing the time evolution of the nuggets is reduced to a differential equation on a single variable $R(t)$.

Our starting point is the observation that the relevant flux which enters equation (2.24) is $\Delta\Phi = (\Phi_{\Rightarrow} - \Phi_{\Leftarrow})$, counting the net baryon charge transfer and sensitive to the chemical potential difference, rather than total flux $\langle\Phi\rangle$ which counts the exchange of all the particles, including bosons[22]. In fact, if the average flux $\langle\Phi\rangle$ were entering equation (2.24) one could explicitly check that this term would be the same order of magnitude as two other terms of the equation. However, the key point is that the baryon charge transfer $\Delta\Phi$ is numerically suppressed, i.e. $\Delta\Phi \ll \langle\Phi\rangle$. In fact, $\Delta\Phi$ identically vanishes for $\mu = 0$. Furthermore, one can use the same technique which has been used in section 2.4.1 to argue that $\Delta\Phi \ll \langle\Phi\rangle$ in entire region of μ. Numerical analysis supports this claim.

To reiterate this claim: while a typical flux defined as

$$\Phi = \frac{g^{\rm in}}{(2\pi)^3}\int \frac{v_z d^3k}{\exp(\frac{k-\mu}{T})+1} + (\text{bosons}) \sim (\text{fm})^{-3} \tag{A.1}$$

assumes a conventional QCD value, the net baryonic flux $\Delta\Phi \cdot S$ through surface S is numerically suppressed, and can be neglected in eq. (2.24).

[22]The dominant contribution to the fluxes normally comes from the lightest degrees of freedom which are the Nambu-Goldstone bosons in hadronic and CS phases. These contributions are crucial for maintaining the thermodynamical equilibrium between exterior and interior, but they do not play any role in the baryon fluxes which enter eq.(2.24).

One can explain this result as follows. Consider a single oscillation of the domain wall evolution. To be more specific, consider a squeezing portion of this evolution when $R(t)$ decreases. During this process the chemical potential (and the baryon charge density) locally grow as we discussed in section 2.4.1. The major portion of this growth is resulted from the baryon charge which was already bound to the domain wall, rather than from the baryon charge which enters the system as a result of the baryonic flux transfer.

On an intuitive level the dominance of the bound charges (accounted in eq. (2.24)) in comparison with flux-contribution (neglected in eq. (2.24)) can be explained using pure geometrical arguments. Indeed, the chemical potential increases very fast as a result of rapid shrinking of the bubble with speed $v \simeq c$. The corresponding contraction of a bubble leads to proportionally rapid increase of the chemical potential on the domain wall. This happens because the baryon charges are strongly bound to the wall, and cannot leave the system due to the topological reasons as the boundary conditions effectively lock the charge to the macroscopically large domain wall. As a result of this evolution the binding energy of a quark $\sim \mu$ increases when the bubble contracts. This process represents a highly efficient mechanism of very rapid growth of the chemical potential due to the domain wall dynamics. It is vey hard to achieve a similar efficiency with the flux-contribution when the probability for a reflection from the domain wall is typically much higher than probability for a transmission. Furthermore, a non-vanishing quark mass make suppression even stronger $\sim \exp(-m/T)$.

To conclude: we do expect that an accounting for the flux- contribution modifies our equations relating $\mu(t)$ and $R(t)$ as expressed by eqs. (2.24), (2.30). However, we do not expect that this modification may drastically change the basic qualitative features of eqs. (2.24), (2.30) which have been heavily employed in this work.

Appendix B

Formation of the Nuggets: Numerical Analysis

This appendix is devoted to exact numerical computation in contrast with analytical qualitative arguments presented in section 2.4. The basic lesson of this Appendix is that a number of simplifications which have been made in section 2.4 are justified, at least, on a qualitative level.

Before we proceed with numerical computations we want to make few comments on parameters entering the basic dynamical equation (2.37). In the previous sections, σ was treated as a constant in order to simplify the analysis. This approximation is justified as long as a typical curvature of the domain wall is much smaller than the width of the domain wall, i.e. $R \gg m_a^{-1}$. This condition is only marginally justified as a typical radius of the bubble is of order m_a^{-1}, which is the same order of magnitude as the width of the wall. At the same time, the width of the QCD substructure of the domain wall (including the η' substructure and the baryon substructure) is very small in comparison with the curvature, and it does satisfy the criteria of a thin wall approximation as $m^{-1} \ll R \sim m_a^{-1}$. Precisely this QCD substructure plays a crucial role in our analysis in section 2.2 where we studied the "local violation" of the baryon charge in the presence of the domain walls. The broad structure of the domain wall due to the axion field with the width m_a^{-1} does not play any role. However, precisely this structure determines the large tension $\sigma \sim m_a^{-1}$ of the domain wall.

We want to effectively account for this physics by assuming that $\sigma(R)$ effectively depends on the radius of the bubble R. On the physical grounds we expect that $\sigma(R)$ approaches its asymptotic value at large R when the domain wall is almost flat, $\sigma(R \to \infty) \to \sigma_0$, while σ reduces its value at smaller R, and eventually vanishes at some cutoff $R_{\rm cut}$. A natural choice is $R_{\rm cut} \simeq 0.24 R_0$ which corresponds to large $\mu_{\rm cut} \lesssim 500$MeV from (2.30), when the chemical potential assumes its typical CS value. To introduce such an infrared cutoff smoothly, it is convenient to parametrize σ as follows

$$\sigma(R) = \sigma_0 e^{-r_0/2(R-R_{\rm cut})} \tag{B.1}$$

where $\sigma_0 \simeq 9 f_a^2 m_a$ is the conventional domain wall tension, see e.g. [11], while r_0 is a free phenomenological parameter, $0 < r_0 \lesssim R_0$ as we expect $\sigma(R_0) \simeq \sigma_0$. In our numerical studies we verified that the physical results (such as formation size $R_{\rm form}$) are not very sensitive to parameter r_0.

Another parameter which requires some comments is the viscosity η. In the context of the present work, the viscosity accounts for a number of different QCD effects which lead to dissipation and "friction". Such effects include, but are not limited to different scattering process by quarks, gluons or Nambu Goldstone Bosons in different phases. Furthermore, the annihilation processes which take place inside the bubble and which result in production of a large number of strongly interacting quasi-particles also contribute to η. The viscosity can be computed from the first principles in weakly coupled quark-gluon phase [71]. However, we are more interested in behaviour of η below T_c. In this case the computations [72] based on chiral perturbation theory suggest that $\eta \sim m_\pi^3$. This numerical value is quite reasonable in all respects, and consistent with simple dimensional arguments. It is also known that $\eta(T)$ depends on temperature [72]. However, we neglect this dependence in our estimates which follow.

Now we can proceed with our numerical studies. Since $\sigma(R)$ is a function of R as explained above, we should start with a modified differential equation for $R(t)$:

$$\begin{aligned} \sigma(R)\ddot{R}(t) &= -\frac{2\sigma(R)}{R} - \frac{\sigma(R)\dot{R}^2}{R} + \Delta P(R) \\ &- (\frac{1}{2}\dot{R}^2 + 1)\frac{d\sigma(R)}{dR} - 4\eta\frac{\dot{R}}{R}. \end{aligned} \tag{B.2}$$

This equation is not identically the same as equation (2.37) discussed in section 2.4. This is due to the fact that the tension $\sigma(R)$ is now become R dependent function as we discussed above. The equation (B.2) has been solved numerically using parameters listed in Table B.1. The numerical values of these parameters can be obviously somewhat modified. However, the basic qualitative features presented in section 2.4 do not drastically change when the QCD parameters are varied within reasonable parametrical region. Our numerical studies, as we discuss below, do support the analytical qualitative results presented in section 2.4.

We start our short description with Fig.B.1. It shows a typical evolution of a bubble with time. The frequencies of oscillations are determined by the axion mass m_a^{-1}, while typical damping time is determined by parameter τ as discussed in section 2.4. To make the pattern of oscillations visible, the

viscosity has been rescaled[23]. At large times, $t \to \infty$, the solution settles at $R_0/R_{\rm form} \simeq 2.9$ and $\mu_{\rm form} \simeq 330{\rm MeV} \sim \mu_1$, consistent with qualitative analysis of section 2.4.

We now describe Fig. B.2 where we zoom-in first few oscillations of a typical solution shown on previous plot Fig. B.1. We want to emphasize that a seeming cusp singularity is actually a smooth function near $R_{\rm min}$. It looks "cuspy" as a result of a large time scale on Fig. B.1. The "cusp" is relatively narrow comparing to macroscopic period of oscillation ($\delta t_{\rm cusp} \sim 10^{-3} R_0$). Nevertheless it actually lasts much longer in comparison with a typical QCD scale ($\delta t_{\rm cusp} \gg \Lambda_{\rm QCD}^{-1}$).

On Fig. B.3 we demonstrate a (non)sensitivity of the system to parameter r_0 introduced in eq. (B.1). One can explicitly see that the initial evolution is indeed quite sensitive to ad hoc parameter r_0. However, the final stage of the evolution is not sensitive to r_0. In other words, the physical parameters $R_{\rm form}$ and τ are not sensitive to ad hoc parameter r_0. Note that estimation of damping time τ and period of oscillation $t_{\rm osc}$ agree well with qualitative estimations presented in section 2.4.

[23] In this plot we use $\eta \simeq 10^8 \eta_0$, which is eight orders of magnitude larger than $\eta_0 \simeq m_\pi^3$. We did it on purpose: First, it simplifies the numerics. Indeed, the η parameter determines the dumping time scale (2.45) which is many orders of magnitude longer than any other scales of the problem. Secondly, we use $\eta \simeq 10^8 \eta_0$ for the demonstration purposes. Indeed, a typical oscillation time ω^{-1} and the damping time τ are characterized by drastically different scales. If we take η according to its proper QCD value than the time scale on plots Fig. B.1 would be eight orders of magnitude longer than shown.

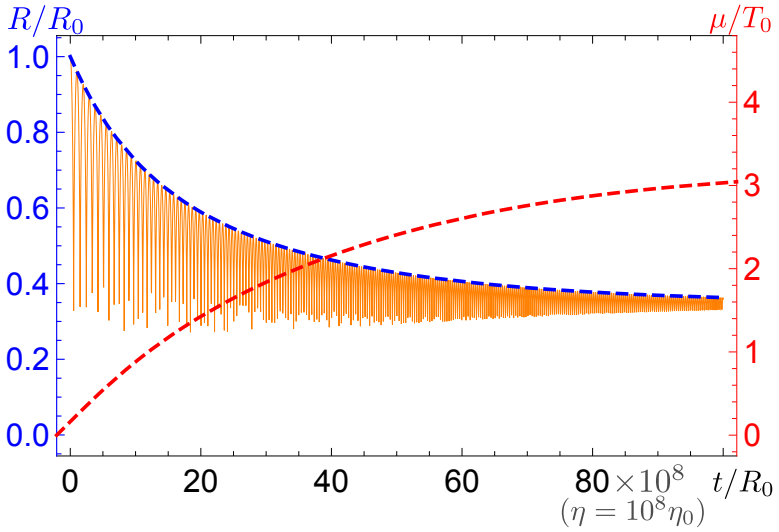

Figure B.1: Typical underdamped solution of $R(t)$ and $\mu(t)$. The oscillations with frequencies $\sim m_a^{-1}$ shown in orange, the modulation of $R(t)$ is shown in blue. The chemical potential $\mu(t)$ shown in red. The initial $R_0 = 10^{11}$fm and $r_0 = 0.5R_0$.

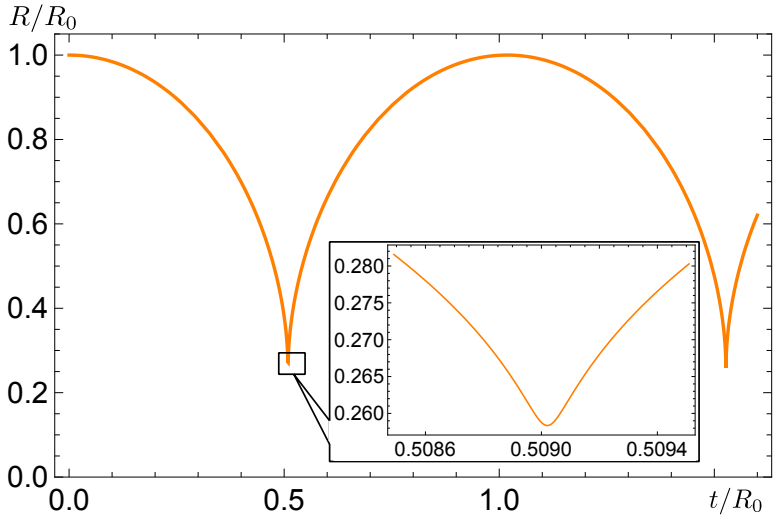

Figure B.2: The first few oscillations of an underdamped solution shown on Fig. B.1.

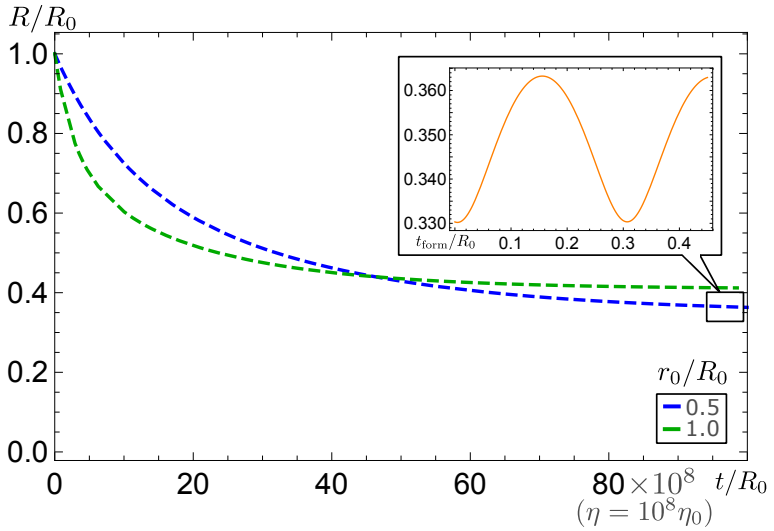

Figure B.3: Dependence on parameter r_0 as defined by eq. (B.1). Zoom-in shows small oscillations during the final stage of formation.

Table B.1: Table for some numerical parameters

Quantity	Symbol	Value	QCD units ($m_\pi = 1$)
flavours	N_f	2	2
colors	N_c	3	3
degeneracy factor (in) (2.21)	$g^{\rm in}$	12	12
degeneracy factor (out) (2.18)	$g^{\rm out}$	37	37
baryon charge on DW (2.12)	N	2	2
axion decay constant	f_a	10^{10}GeV	7×10^{10}
mass of axion	m_a	6×10^{-4}eV	4×10^{-12}
domain wall tension	σ_0	5×10^8GeV^3	2×10^{11}
bag constant (2.23)	E_B	$(150\text{MeV})^4$	1.5
"squeezer" parameter (2.23)	μ_1	330 MeV	2.4
cosmological time scale	t_0	10^{-4}s	10^{19}
initial μ	μ_0	1.35 MeV	0.01
initial radius	R_0	10^{-2}cm	10^{11}
initial temperature	T_0	100 MeV	0.74
QCD viscosity[72]	η_0	0.002 GeV^3	1

Appendix C

Evaluation of Fermi-Dirac Integrals

The main goal of this Appendix is to present some supporting arguments suggesting that the approximation we have used in section 2.4.1 and which involves the Fermi-Dirac integrals are qualitatively justified. Indeed, the relevant integrals which enter eqs. (2.28), (2.31) have the form

$$I_n(b) \equiv \int_0^\infty \frac{dx \cdot x^{n-1}}{e^{x-b}+1}, \quad b = \frac{\mu}{T} > 0, \tag{C.1}$$

where $n = 2$ appears in integral (2.28), while $n = 4$ appears in (2.31). We will hence focus on evaluation of I_2 and I_4 in this appendix. They can be exactly evaluated as

$$I_2(b) = \frac{\pi^2}{6} + \frac{1}{2}b^2 + \mathrm{Li}_2(-e^{-b}) \tag{C.2a}$$

$$I_4(b) = \frac{7\pi^4}{60} + \frac{\pi^2}{2}b^2 + \frac{1}{4}b^4 + 6\,\mathrm{Li}_4(-e^{-b}) \tag{C.2b}$$

where $\mathrm{Li}_2(-z)$ and $\mathrm{Li}_4(-z)$ are the polylogarithm functions of order 2 and 4, respectively. Polylogarithm functions are commonly known to represent the Fermi-Dirac and Bose-Eisterin integrals. The Polylogarithm functions are defined as

$$\mathrm{Li}_n(-z) = \sum_{k=1}^{\infty} \frac{(-1)^k}{k^n} z^k. \tag{C.3}$$

Note that $|z| = e^{-b} \leq 1$ for any positive b. In this case $\mathrm{Li}_n(-z)$ is evidently fast-converging, so that we can efficiently estimate it by extracting the leading exponent e^{-b} then using the Taylor expansion for the remaining piece:

$$\mathrm{Li}_2(-e^{-b}) \simeq e^{-b}\left[-\frac{\pi^2}{12} + (\ln 2 - \frac{\pi^2}{12})b + \mathcal{O}(b^2)\right]$$

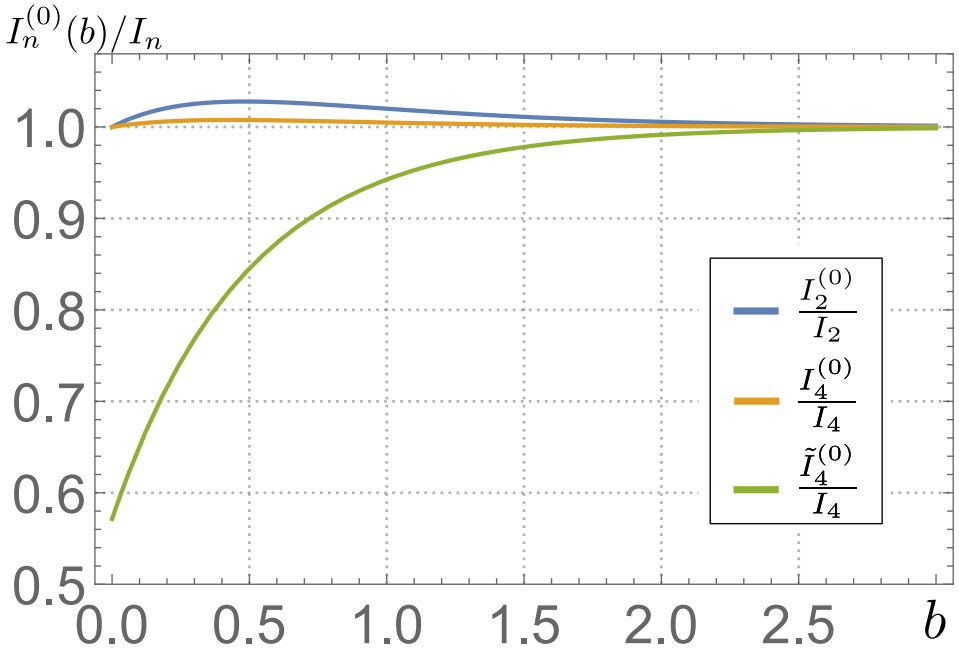

Figure C.1: Comparison of $I_n^{(0)}$ to I_n with different values of b.

$$\mathrm{Li}_4(-e^{-b}) \simeq e^{-b}\left[-\frac{\pi^4}{720} + (\frac{3\zeta(3)}{4} - \frac{7\pi^4}{720})b + \mathcal{O}(b^2)\right],$$

where $\zeta(3) \simeq 1.202$ is the Riemann zeta function. Neglecting the terms of order $\mathcal{O}(be^{-b})$ which are small in both limits, at large and small chemical potentials, one can approximate I_2 and I_4 as follows

$$I_2^{(0)} \simeq \frac{\pi^2}{6} + \frac{1}{2}b^2 - \frac{\pi^2}{12}e^{-b} + \mathcal{O}(be^{-b}) \tag{C.5a}$$

$$I_4^{(0)} \simeq \frac{7\pi^4}{60} + \frac{\pi^2}{2}b^2 + \frac{1}{4}b^4 - \frac{7\pi^4}{120}e^{-b} + \mathcal{O}(be^{-b}). \tag{C.5b}$$

We test our approximation by comparing our approximate expressions (C.5a), (C.5b) with exact formulae (C.2a), (C.2b). As one can see from Fig. C.1, our approximation shown in blue ($I_2^{(0)}/I_2$) and orange ($I_4^{(0)}/I_4$) is very good with errors less than 3% in the entire range of $b > 0$.

On the same plot we also show the approximation $\tilde{I}_4^{(0)}$ for approximate

expression $I_4^{(0)}$ used in the main text in eq. (2.31)

$$\tilde{I}_4^{(0)} \simeq \frac{7\pi^4}{60} + \frac{\pi^2}{2}b^2 + \frac{1}{4}b^4 - \frac{\pi^4}{12}e^{-b}. \tag{C.6}$$

The error for $\tilde{I}_4^{(0)}$ is quite large for very small chemical potential $b \ll 0.5$, on the level of 40%, shown in green. The error becomes much smaller after short period of time when $b = \mu/T \geq 0.5$ becomes sufficiently large. To conclude: the approximations of the integrals in section 2.4.1 are sufficiently good for qualitative analysis presented in that section.